Journal of Quantitative Spectroscopy & Radiative Transfer 316 (2024) 108897

Contents lists available at ScienceDirect

Journal of Quantitative Spectroscopy and Radiative Transfer

journal homepage: www.elsevier.com/locate/jqsrt

Empirical rovibrational energy levels for methane

Kyriaki Kefala [a], Vincent Boudon [b], Sergei N. Yurchenko [a], Jonathan Tennyson [a,*]

[a] Department of Physics and Astronomy, University College London, Gower Street, London WC1E 6BT, UK
[b] Laboratoire Interdisciplinaire Carnot de Bourgogne, UMR 6303 CNRS-Université de Bourgogne, 9 Avenue Alain Savary, BP 47870, F-21078 Dijon Cedex, France

ARTICLE INFO

Keywords:
Rovibrational energy levels
MARVEL
Methane
$^{12}C^{1}H_4$
Line list
ExoMol

ABSTRACT

A MARVEL (Measured Active Rotational Vibrational Energy Levels) analysis of the available spectroscopic data on methane ($^{12}C^{1}H_4$) is performed. A total of 82173 measured rovibrational transitions were gathered from 96 literature sources and put through the MARVEL procedure which led to the determination of 23292 empirical energy levels with uncertainties, up to 9900 cm^{-1} covering the lowest eight polyads. A comparison with Effective Hamiltonian evaluated levels, variational calculations by the TheoReTS project, and the MeCaSDa database is performed. The new levels generated will be used to improve the upcoming ExoMol MM line list.

1. Introduction

Methane ($^{12}C^{1}H_4$) is the simplest stable hydrocarbon molecule, with wide-ranging implications in atmospheric and astrophysical chemistry. Methane on Earth has, natural, biological, and geological origins. It is produced by methanogenic microorganisms on wetlands as a metabolic byproduct. A natural reservoir of methane exists under permafrost regions and underneath the oceans in the form of methane hydrates [1]. Methane is central in atmospheric chemistry and its presence in the atmosphere affects the planet's temperature and climate system. Methane's concentration in the troposphere is increasing after a decade of constant value [2,3] making it an important global warming species. It has been identified as the second anthropogenic greenhouse gas after carbon dioxide [4,5]. Methane's atmospheric lifetime is notably shorter than that of carbon dioxide, primarily due to its reactivity with hydroxyl radicals (OH). Despite its shorter lifespan, methane is a more potent greenhouse gas, contributing significantly to heat-trapping in the atmosphere [4]. Consequently, precise measurement and monitoring of methane concentrations are of paramount importance for researchers dedicated to combating climate change [6]. Global methane emissions stem from a variety of human activities, surpassing those originating from natural processes. These anthropogenic sources include emissions from agriculture, biomass burning, the gas and oil industry, large-scale deforestation, industrial processes, combustion, and wastewater treatment, among others. In contrast, the number of natural methane sinks remains limited [7].

Methane's role in atmospheric chemistry and climate impact is not limited to Earth; methane is notably abundant within our Solar System [8]. Primarily found on the outer planets, methane is prevalent in the atmospheres of Jupiter [9], Saturn [10], Uranus [11], and Neptune [12]. It has also been detected on Venus [13] and several moons, including Titan [14–16] and Triton [17–20], which renders it invaluable for atmospheric analysis and modeling. In addition to these celestial bodies, methane has sparked extensive debates regarding its presence and significance on Mars [21–26], as well as its origin on the Martian surface [27]. Moreover, methane has been detected in some distant objects like comets [28,29] by flyby missions and ground observations, as well as Pluto [30]. Infrared absorption spectra of Type *T* class of brown dwarfs also reveal the presence of methane [31,32] and are even referred to as "methane dwarfs" [33].

Our primary focus in this study is the significance of methane in the investigation of extrasolar planets. High-resolution infrared spectroscopy is very important in order to understand the chemical composition of the atmosphere of such planets [34]. The substantial advancements in exoplanet discovery have ignited a strong interest within the scientific community to identify exoplanets that may be inhabited or possess habitable conditions. Therefore, recognizing and detecting biosignatures is one of the main goals of researchers in this field. Methane is considered a biosignature for terrestrial planets [35,36], which means it can be a very good indicator of the presence of life beyond Earth, and maybe a sign of early Earth-like environments. Interestingly, it is the sole detectable biosignature by the James Webb Telescope, in contrast to oxygen [37].

In the context of exoplanets, gas giants known as hot Jupiters are expected to contain methane, alongside other molecules such as water and carbon monoxide [38]. Indeed, methane has been observed in the atmospheres of hot, gaseous exoplanets, including HD 189733b, HD 209458b, and XO-1b [34,39–41]. Furthermore, warm Neptunes like GJ 436b and GJ 3470b are expected to exhibit methane-rich atmospheres,

* Corresponding author.
E-mail addresses: kyriaki.kefala.20@ucl.ac.uk (K. Kefala), j.tennyson@ucl.ac.uk (J. Tennyson).

https://doi.org/10.1016/j.jqsrt.2024.108897
Received 3 December 2023; Received in revised form 30 December 2023; Accepted 3 January 2024
Available online 11 January 2024

although its abundance on these planets has occasionally been a subject of debate [42–45]. Consequently, accurately determining the methane content is essential for characterizing exoplanets [46,47].

The importance of methane has led to the construction of numerous line lists [48–55], and plenty of experimental works aimed at accurately characterizing methane's spectral properties. A large number of such works have been utilized in the current analysis. In this work, we compiled all the available experimental spectroscopic data up until July 2023 and put them through the MARVEL procedure in order to determine a dataset of empirical rovibrational energy levels with experimental accuracy. The goal is to improve the upcoming ExoMol MM methane line list [56] by using empirical energy levels in place of the computed values with the variational program TROVE [57].

2. Theoretical background

2.1. MARVEL

Furtenbacher et al. developed the Measured Active Rotation Vibration Energy Level (MARVEL) algorithm [58–61] that we use here to determine accurate empirical energy levels of $^{12}C^{1}H_4$. The MARVEL procedure starts with the creation of a dataset of measured high-resolution spectroscopic transition frequencies (line positions). It is essential that the transitions are assigned with a consistent set of quantum numbers for their upper and lower states and have uncertainties. Each transition is labeled uniquely with a tag that shows the source it originates from, as well as a number identifying it within the source.

MARVEL employs a methodology of transition inversion to derive a set of empirical energy levels accompanied by their respective uncertainties via a weighted linear least-squares inversion protocol. This process involves a meticulous evaluation of the self-consistency of experimental transition frequencies, followed by iterative adjustments of uncertainty values. The goal is to attain a cohesive network of energy levels, referred to as a spectroscopic network. In this network, vertices represent discrete energy levels, and edges represent the transitions connecting these levels [62–64]. Specifically, MARVEL computes optimal uncertainty values for each energy level to ensure their internal consistency within the spectroscopic network.

The MARVEL 4 Online version [65] offers enhanced flexibility in handling transition energy units. Unlike previous versions that exclusively used cm^{-1}, Marvel 4 Online can accommodate various units (cm^{-1}, Hz, kHz, MHz, GHz, and THz). To support this expanded functionality, a segment file is included as an input, containing a list of source names paired with their respective units.

MARVEL helps enhance significantly the quality of the database by identifying outliers, often resulting from inaccurately assigned wavenumbers or during the transcription of the measured data into the transition list. Transitions are flagged as invalid if the ratio between the optimal uncertainty and the original uncertainty exceeds a threshold of 100. These invalidated transitions are either corrected or annotated with a negative sign applied to their wavenumber values, to exclude them from further analysis by MARVEL.

By iteratively applying this procedure, we systematically improve the transition uncertainties while simultaneously removing incorrect lines from the database. This process results in the compilation of a catalog of uniquely labeled and internally consistent transitions, which subsequently serves as the foundation for generating the MARVEL energy levels.

It is challenging to find the optimal set of transition uncertainties since they are experimental, and we usually need to increase them manually in order to create a self-consistent network. However, MARVEL offers a feature known as the bootstrap method, which iteratively performs calculations to determine the optimal energy level uncertainties [65]. With the bootstrap method, however, the uncertainties of the final set of MARVEL uncertainties are determined to be suitable and reasonable. In this work, we performed the analysis both with and without the bootstrap method.

2.2. Quantum numbers and selection rules

Methane is a spherical top molecule with tetrahedral symmetry and belongs to the symmetry group T_d with five irreducible representations A_1, A_2, E, F_1, and F_2 [66]. It has nine vibrational degrees of freedom and four normal modes of vibration: The non-degenerate symmetric C–H stretching vibration ν_1 (A_1 symmetry), the doubly degenerate C–H bending vibration (E symmetry) known as the ν_2 mode, and two triply degenerate modes (F_2 symmetry); the ν_3 mode corresponds to the C–H stretching vibration, while the ν_4 mode is associated with the C–H bending vibration. Each vibrational level is identified by a set of nine normal quantum numbers: v_1, v_2, v_3 and v_4 describing the corresponding excitations of the four normal modes ν_1, ν_2, ν_3 and ν_4, and l_2, l_3 and l_4, describing the vibrational angular momenta of ν_2, ν_3 and ν_4, as well as the associated multiplicity indices m_3 and m_4 [50]. The fundamental frequency wavenumbers are $\tilde{\nu}_1(A_1) = 2916.481\ cm^{-1}$, $\tilde{\nu}_2(E) = 1533.333\ cm^{-1}$, $\tilde{\nu}_3(F_2) = 3019.493\ cm^{-1}$, $\tilde{\nu}_4(F_2) = 1310.761\ cm^{-1}$ [67].

The four normal mode wavenumbers $\tilde{\nu}_i$ exhibit the following approximate relation:

$$\tilde{\nu}_1 \simeq \tilde{\nu}_3 \simeq 2\tilde{\nu}_2 \simeq 2\tilde{\nu}_4 \simeq 3000\,cm^{-1}. \quad (1)$$

This leads to the vibration energies of methane being grouped in a polyad structure [68,69]. The integer polyad number P is defined as $P = 2(v_1 + v_3) + v_2 + v_4$ and is numbered with increasing energy starting with $n = 0$ for the Monad, $n = 1$ for the Dyad, $P = 2$ for the Pentad, $P = 3$ for the Octad, *etc*. Fig. 1 shows schematically the first eight polyads of methane with the number of levels and sublevels within each one. Each polyad is labeled with a Greek prefix for the number of the levels. Here a vibrational level is defined simply by the quantum numbers (v_1, v_2, v_3, v_4) while the sublevels comprise all the vibrational angular momentum or symmetry products that are allowed for this vibrational level. Thus, the vibrational level (v_1, v_2, v_3, v_4) is split into several sublevels as soon as it is not just one fundamental level. For instance, "$2\nu_3$" or level (0, 0, 2, 0) has three sublevels A_1, E and F_2. The degeneracy exhibited by three of the normal modes results in an increasing number of vibrational sublevels as the molecule is excited.

In addition to the vibrational quantum numbers, the total angular momentum of the molecule is denoted J. Methane is classified into three nuclear spin isomers: meta ($I = 2$, A_1, A_2), ortho ($I = 1$, F_1, F_2) and para ($I = 0$, E). In the case of higher polyads, the number of sublevels m within a particular symmetry species tend to closely approximate a regular representation, with a ratio of $m(A_1) : m(A_2) : m(E) : m(F_1) : m(F_2)$ equal to 1:1:2:3:3 [67].

The full assignment using the normal mode quantum numbers albeit being theoretically most appropriate gets quickly very complicated with the vibrational excitations. As a practical alternative, the following set of four rotation-vibration quantum numbers is used: the polyad number P, the total angular momentum J, the total symmetry C, the counting number α, which counts the levels with the same (C, J) within a polyad from lower to higher energy.

The electric dipole transitions follow specific selection rules determined by their symmetry:

$$A_1 \leftrightarrow A_2\ , E \leftrightarrow E\ , F_1 \leftrightarrow F_2$$

with the standard rotational angular momentum selection rules:

$$\Delta J = -1, 0, 1, \quad J' + J'' \neq 0,$$

leading to the three well-known P, Q and R branches, respectively.

The symmetric ν_1 stretching (A_1) and the asymmetric ν_2 bending (E) modes lead to no change in the dipole moment and as such, are infrared inactive. Only the two F_2 modes ν_3, ν_4 (and more generally, all F_2 vibrational sublevels) are infrared active for transitions starting in the ground vibrational state, as a first approximation. The ro-vibrational transitions of the IR non-active bands get intensities through ro-vibrational interactions with IR active states.

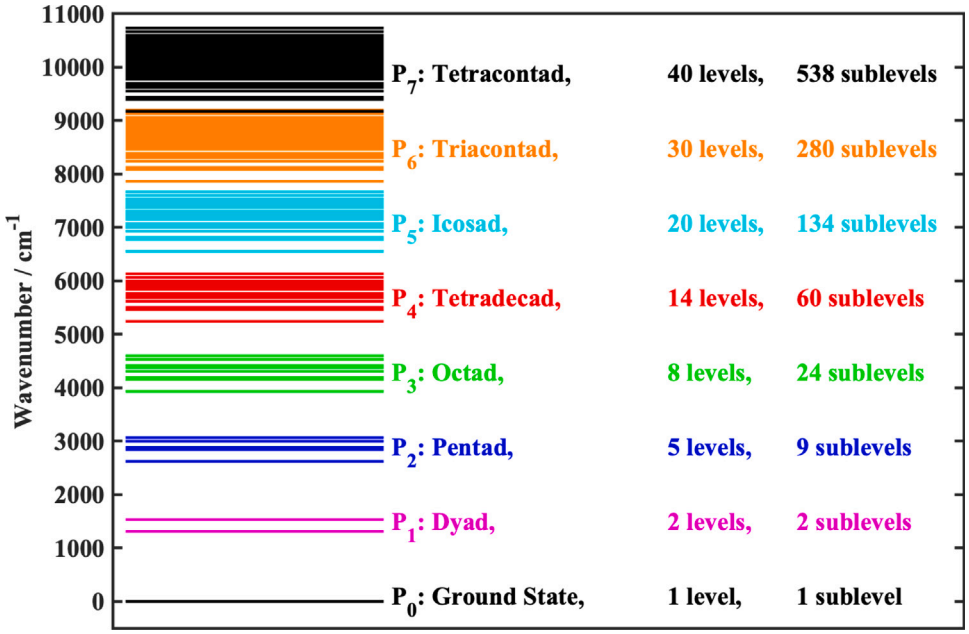

Fig. 1. The first eight vibrational polyads of methane and the number of vibrational levels and sublevels in each one [70].

Table 1
Information on the number of experimental sources and transitions per vibrational band included in our input line list. Average uncertainty is given in cm^{-1}. A/V: total number of available transitions/number of validated transitions.

Bands	A/V	Sources	Av. Unc. cm^{-1}
*P*0–*P*0	153/153	10[a]	0.002262
*P*1–*P*0	3452/3433	12	0.008287
*P*1–*P*1	140/140	4	0.002144
*P*2–*P*0	3406/3397	29	0.003453
*P*2–*P*1	5932/5931	6	0.003850
*P*2–*P*2	16/16	2	0.000001
*P*3–*P*0	32369/32308	13	0.006160
*P*3–*P*1	1699/1699	1	0.002000
*P*3–*P*2	149/149	2	0.001907
*P*4–*P*0	21154/21028	21	0.002323
*P*4–*P*1	7316/7275	3	0.007303
*P*4–*P*2	31/17	3	0.015161
*P*4–*P*3	44/34	1	0.002000
*P*5–*P*0	5953/5927	8	0.001381
*P*5–*P*1	22/22	1	0.001000
*P*6–*P*0	329/329	1	0.005000
*P*6–*P*2	26/26	2	0.003492
*P*7–*P*3	4/2	1	0.005000

[a] One of them is "magic" numbers explained in Section 4.1.

In this analysis, we have used transitions both from Raman and infrared spectra. The selection rules for the Raman spectrum of methane follows: all four vibrational modes are active and the rotational selection rules in the general case are:

$$\Delta J = -2, -1, 0, 1, 2,$$

leading to the five O, P, Q, R and S branches. One should notice however that for the A_1 vibrational sublevels, such as ν_1 fundamental band, there is only a Q Raman branch ($\Delta J = 0$).

3. Overview of experimental sources

A comprehensive collection of high-resolution spectra of $^{12}C^{1}H_4$ has been assembled for this study. A total of 279 research articles were reviewed, and from this pool, 96 were selected for inclusion in our current research. A summary of these selected sources, along with details regarding their observational data, is presented in Tables 1 and 3. Additionally, Table 4 provides information about the sources that were considered but ultimately excluded from our analysis. Comments related to Table 3, especially referring to the assignment of unassigned lines and the treatment of the uncertainties are found in Section 3.1.

We built the dataset of the observational spectra from lower to higher polyads testing with MARVEL at each step. In particular, for our final runs, we used the MARVEL 4 Online version [65].

3.1. Comments on the data sources

During the MARVEL process, we increased some initial uncertainties to create a self-consistent network. We also estimated uncertainties when they were missing in the original papers. Regarding the line assignments, many sources had fully assigned lines, while others did not. For those without assignments, we either assigned them ourselves or excluded them. This subsection provides detailed notes and comments on sources for which full assignments were unavailable in the source data.

76Pine [71]: The transitions were assigned in the paper using a different counting numbers convention. We reassigned them using the Effective Hamiltonian fit by 16AmLoPi [72].

79DaPiRo [73]: We assigned the counting numbers using transitions from other sources.

79PiDu [74]: The ν_4 transitions are assigned using a different convention for the counting numbers in the original paper, and we reassigned them using lines from [75] and the set of calculated energy levels provided by 16AmLoPi [72].

82JeRo [76]: The ν_4 transitions are partly assigned in the original paper without the upper state's counting numbers. We were able to assign them using the Effective Hamiltonian fit by 16AmLoPi [72].

16AmLoPi [72]: We used the P_1–P_0 and P_2–P_1 lines but not the P_3–P_2, P_4–P_3 lines because they were inconsistent with the rest of the network.

83DeFrPr and **83DeFrPrb** [77,78]: The lines were taken as published and assigned by 97MaBeSa [79].

85ChKlNi [80], **79DoKoTa** [81], and **81DoKoTa** [82]: Measurements of one F-symmetry line at 88 THz were published by 85ChKlNi [80]. The original papers 79DoKoTa [81] and 81DoKoTa [82] (references 6 and 8 of [80] respectively) were not found. Other measurements of the same transition were published by 82ChGoKl [83], 76BlEdJo [84], 80KnEdPe [85], 80ClDaRu [86], 72EvDaWe [87], and 92KrLiWe [88] and we assigned them fully using lines by 09AlBaBo [70].

88Brown [89]: 12 of the 235 published observed transitions were identified as $3\nu_4$ R0-R4 lines. We assigned the quantum numbers for these lines using the Effective Hamiltonian fit by 16AmLoPi [72].

92PuWe [90]: We assigned the counting numbers for the pure rotational transitions in the ν_3 band with the use of the calculated energies from the Effective Hamiltonian fit by 16AmLoPi [72].

98BrKaRu [91]: We used the more recent assignments from [72].

98ErTyKr [92]: One E-line is measured, which we assigned fully using [70].

00FeChJo [93]: The upper state's counting numbers were assigned using 09AlBaBoBr [70] lines.

02HiQu [94]: The full assignments were taken from 12TaQu [95].

05Brown [96]: The full assignments of 27 of the published lines were taken from 12TaQu [95].

05PrBrMa [97]: We reassigned the following transitions:

4286.949 cm^{-1} from ($P'=3$, $J'=4$, $C'=F_2$, $\alpha'=41$; $P''=0$, $J''=5$, $C''=F_1$, $\alpha''=1$) to (3, 4, F_2, 41; 0, 5, F_1, 2),

4509.857 cm^{-1} from (3, 10, A_1, 37; 0, 9, A_2, 1) to (3, 10, A_2, 35; 0, 9, A_1, 1),

4492.216 cm^{-1} from (3, 4, F_2, 52; 0, 3, F_1, 1) to (3, 4, F_2, 58; 0, 5, F_1, 1),

4522.050 from (3, 11, F_1, 117; 0, 10, F_2, 3) to (3, 11, F_2, 114; 0, 10, F_1, 2).

09ScKaGa [98]: Full assignments of 27 of the published lines were taken from 12TaQu [95].

10NiLyMi [99]: We assigned the upper state's counting numbers of 2551 lines using lines from 15NiLyMi [51] as well as lines from other sources in this range.

12CaWaMo [100]: The transitions were published unassigned, and we used the assignments provided in the HITRAN database [101].

12TaQu [95]: We attributed the counting numbers using HITRAN lines [102], and lines from [103], and [94].

13AbIwOk [104]: The full assignments were taken from 18AmBo [105].

13CaLeWa [106]: The transitions were published unassigned, but have been assigned in other works; we used 3436 lines assigned by 17NiChRe [107], and 2445 lines by 16NiReTa [108]. In addition, 16ReNiCa [109] published 10034 partly assigned lines in the range 6539–6800 cm^{-1} without counting numbers. We assigned counting numbers for 1906 of these lines using other sources. We also reassigned the following lines after evaluating them with MARVEL:

5931.350 cm^{-1} from (4, 8, F_1, 207; 0, 7, F_2, 1) to (4,8, F_1,208;0,7, F_2,1),

6102.645 cm^{-1} from (4, 10, F_2, 325; 0, 9, F_1, 3) to (4, 10, F_2, 326; 0, 9, F_1, 3),

5998.240 cm^{-1} from (4, 10, F_2, 325; 0, 10, F_1, 2) to (4, 10, F_2, 326; 0, 10, F_1, 2).

13NiBoWe [110]: We reassigned the following transition: 5782.556 cm^{-1} from (4, 8, F_2, 180; 0, 8, F_1, 1) to (4, 8, F_2, 181; 0, 8, F_1, 1).

13ZoGiBa [111]: 1153 assigned lines were published with no counting number for the upper state. We assigned 348 of them using the Effective Hamiltonian fit by 16AmLoPi [72].

16DeMaRe [112]: 307 assigned lines were published without the upper state's counting numbers. We attributed the counting numbers using the Effective Hamiltonian fit by 16AmLoPi [72].

17HaPrNi [113]: We reassigned the following transitions:

4417.888 cm^{-1} from (3, 7, F_1, 66; 0, 6, F_2, 1) to (3, 7, F_1, 66; 0, 6, F_2, 2),

4489.943 cm^{-1} from (3, 4, F_2, 56, 0, 5, F_1, 1) to (3, 4, F_2, 56; 0, 5, F_1, 2),

4469.327 cm^{-1} from (3, 6, F_2, 80, 0, 7, F_1, 1) to (3, 6, F_2, 80; 0, 7, F_1, 2),

4432.663 cm^{-1} from (3, 8, F_2, 76; 0, 7, F_1, 1) to (3, 8, F_2, 76; 0, 7, F_1, 2),

4427.818 cm^{-1} from (3, 8, F_2, 75; 0, 7, F_1, 1) to (3, 8, F_2, 75; 0, 7, F_1, 2).

18GhMoKa [114]: We reassigned the transition 5753.757 cm^{-1} from (4, 8, F_1, 207; 0, 9, F_2, 1) to (4, 8, F_1, 208; 0, 9, F_2, 1).

18GoPrKa [115]: The counting numbers were attributed using the lines by 16DeMaRe [112].

18KoMaEs [116]: We assigned counting numbers using lines by 13TyTaRe [117].

18YaLiFe [118]: Lines from several other sources were used to attribute counting numbers.

19LiYaFe [119]: We attributed full assignments using HITRAN lines [102] or the Effective Hamiltonian fit by 16AmLoPi [72].

19YaLiFe [120]: One measured transition is published in this work and assigned as an $R(1)$ $2\nu_1+\nu_3$ line. We reassigned this line to an $R(0)$ line and assigned counting numbers using the HITRAN database [102], and the sources 13ZoGiBa [111] and 13CaLeWa [121].

20YaLiPl [122]: We assigned 6 of the published lines using transitions from several other sources.

21OkInOk [123]: The counting numbers for the transitions were found using lines from other sources and the Effective Hamiltonian fit by 16AmLoPi [72].

21FoRuSi [124]: The full assignments for the transitions were attributed using other lines from our line list, as well as calculated energies from 16AmLoPi [72].

3.2. Raman spectra

The following data sources provided Raman spectra we evaluated and considered in our analysis.

Table 2
Magic numbers. Wavenumber values were selected from the effective Hamiltonian energy values by 16AmLoPi [72].

Wavenumber cm^{-1}	Unc cm^{-1}	Upper state				Lower state				Label
		P'	J'	C'	α'	P''	J''	C''	α''	
10.481641	0.000001	0	1	F_1	1	0	0	A_1	1	MAGIC.1
31.442100	0.000001	0	2	E	1	0	0	A_1	1	MAGIC.2
31.442366	0.000001	0	2	F_2	1	0	0	A_1	1	MAGIC.3
62.878129	0.000001	0	3	A_2	1	0	0	A_1	1	MAGIC.4
104.772781	0.000001	0	4	A_1	1	0	0	A_1	1	MAGIC.5
62.875738	0.000001	0	3	F_1	1	0	0	A_1	1	MAGIC.6
2179.816	0.030	0	20	E	1	0	0	A_1	1	MAGIC.7
2620.967	0.010	0	22	E	1	0	0	A_1	1	MAGIC.8
3104.763	0.010	0	24	A_2	1	0	0	A_1	1	MAGIC.9
3104.752	0.010	0	24	F_2	2	0	0	A_1	1	MAGIC.10

We included 379 Raman transitions in total. The sources we used are the following:

75ChBe [125] reported 196 ν_2 Raman transitions in the range 1360–1770 cm^{-1} belonging to the O, P, R, and S branches which were assigned by 76GrRo [126] and 77Champion [127].

92BeSaCa [128] reported 83 ν_1 and $\nu_2 + \nu_4$ Raman lines in the range 2911–2921 cm^{-1} belonging in the Q branch.

91MiLaSt [129] reported 13 ν_2 Raman lines in the range 3063–3066 cm^{-1} belonging to the Q Branch.

94HiChTo [130] reported 37 $2\nu_2$ Raman lines in the Q branch and the range 3063–3070 cm^{-1} from a thesis by J.M. Jouvard, University of Bourgogne (1991).

97MaBeSa [79] measured 21 $2\nu_1 - \nu_1$ Raman lines in the Q branch. In addition, they reported 4 Raman lines in the $2\nu_3 - \nu_3$ band in the R and P branches and the 2800–6000 cm^{-1} range that are originally from 83DeFrPr [77], as well as 6 lines from 83DeFrPrb [78]. The 83DeFrPrb lines were not validated by MARVEL.

92SaCaDo [131] reported 45 ν_1 Raman lines that have also been published and assigned by 92BeSaCa [128], as well as 13 lines by 79KoPrSm [132] and 6 lines by 85GrLa [133]. The assignments of these lines were also done using lines by 92BeSaCa [128].

The following Raman sources were not used:

85ThFaKo [134]: The Raman lines reported were not used because of low accuracy.

78OwPaDo [135]: 32 ν_1 Raman lines were measured in the 2916–2918 cm^{-1} range with assignments without counting numbers.

70ClSt [136]: No measured wavenumbers.

75Champion [137]: Only calculated values were provided.

78MaHeBy [138]: No measured wavenumbers.

15MaKcVa [139]: Measured Raman spectra were reported at temperatures ranging from 300 K to 860 K covering the 882 – 1791 cm^{-1} and 2548 – 3434 cm^{-1} regions without assignments.

77Berger [140]: Raman ν_3 lines were reported ranging from 2850 cm^{-1} to 3100 cm^{-1}. The lines were assigned in this source as well as by [141] but the counting numbers follow a different convention that we could not use.

83FrIlFi [142]: ν_1 Raman Q branch lines were reported from 2916 to 2917 cm^{-1} assigned with a different convention for the counting numbers.

06JoChSa [143]: No measured wavenumbers.

82LoBrRo [144]: Measurements of $2\nu_4$ Raman transitions in the 2460–2675 cm^{-1} region were published. The assignments were different and due to low accuracy, we were not able to include them in the analysis at this stage.

07JoGaCh [145]: No measured wavenumbers.

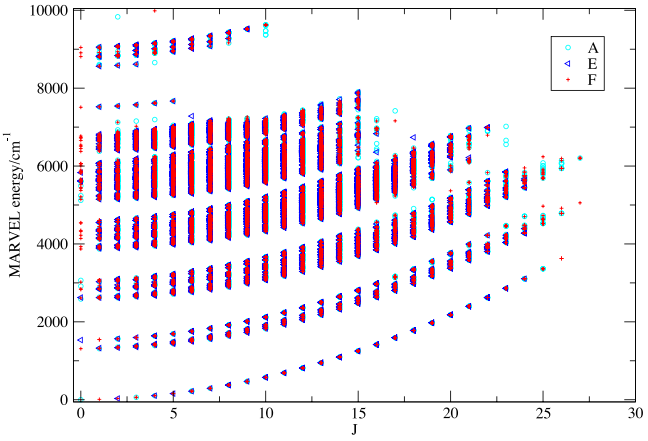

Fig. 2. The $^{12}C^1H_4$ MARVEL energy levels for the first eight polyads obtained in this work. The symbols denote the different symmetries; A: A_1, A_2, E: E, F: F_1, F_2.

4. The MARVEL networks

Out of a total of 82173 transition frequencies assessed by the MARVEL procedure, 308 were not validated and were assigned a negative wavenumber in the input line list. At this stage, six artificial transitions were included called "magic" numbers (the first six in Table 2). Three of them to connect the different nuclear spin isomers, and three to improve the network connectivity as explained below in Section 4.1. This resulted in a spectroscopic network comprising 81865 lines, separated into 305 components. The largest component consisted of 80598 transitions connecting 23060 energy levels, with 109 of these components containing one single transition linking two levels.

The next four components were two E symmetry, one A_1/A_2, and one F_1/F_2 symmetry networks which consisted of 103, 57, 48, and 44 transitions respectively. To establish connections between them and the largest component four new magic numbers were added (the last four in Table 2). We connected only these four to the largest network because the next was a much smaller one consisting of only 29 transitions. As a result, we ended up with 81872 validated transitions in total separated into 301 components, the largest one of which includes 80854 transitions that link 23292 energy levels.

The distribution of energy levels according to their symmetries is as follows: 21.4% are of A_1/A_2 symmetry, 18.4% are of E symmetry, and 60.2% are of F_1/F_2 symmetry. The energy distribution with respect to J are illustrated in Fig. 2 and relevant details are given in Table 5.

We compared our empirical rovibrational energy levels to the Effective Hamiltonian results of 16AmLoPi [72], variational energies from the TheoReTS project [53], and calculated levels from the MeCaSDa database [146]. Figs. 3 and 4 show the differences between the MARVEL levels and levels from the TheoReTS project. For the comparison with the MeCaSDa database see the Supplementary Material,

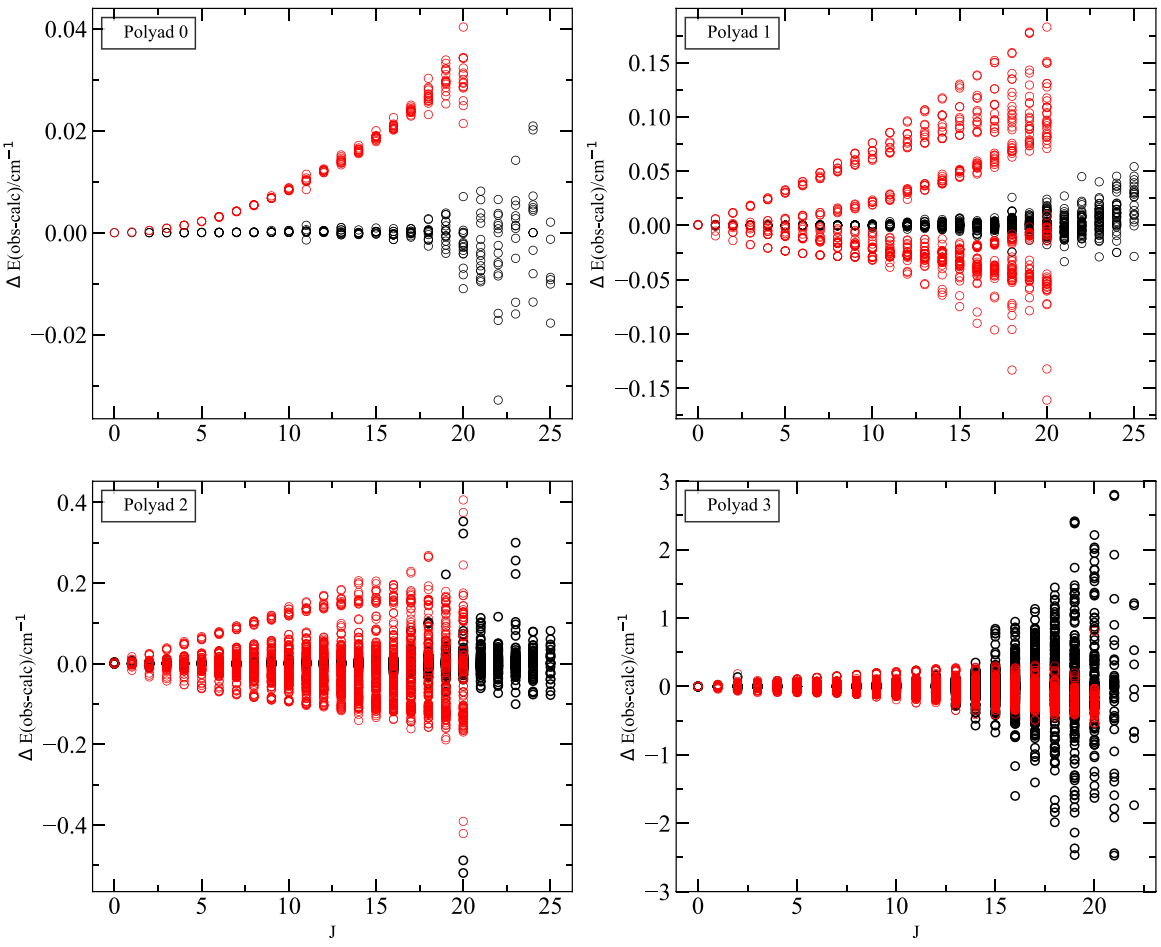

Fig. 3. Difference between the MARVEL energies (obs) and the a. Effective Hamiltonian by [72] (black) b. Variational calculations (red) by [53].

which also provides the full comparison with the TheoReTS variational calculations.

For the first two polyads the agreement with the Effective Hamiltonian energies by 16AmLoPi [72] is very good for $J \leq 17$ with a maximum difference of less than 0.007 cm^{-1}. For the next two polyads, the agreement with the Effective Hamiltonian energies is very good for $J \leq 15$ with a maximum difference of less than 0.014 cm^{-1}. Regarding the comparison with the TheoReTS variational energies, the agreement is always within 1 cm^{-1} for the first five polyads. Additionally, in polyad 3 the TheoReTS energies exhibit better agreement with the MARVEL energies than the Effective Hamiltonian energies in high J values. The comparison with the MeCasDa database follows a similar trend to the one with the Effective Hamiltonian results. The differences grow with J and polyad P in all cases and grow more in the cases of polyad 5 and polyad 6 where our data are limited.

For polyad 2 Fig. 3 shows a difference of $\simeq$ 0.4 cm^{-1} between MARVEL and the Effective Hamiltonian energies, as well as the TheoReTS energies for four $J = 20$ levels. These differences are much smaller when compared with MeCaSDa (see Supplementary Material). These four levels, comprising two E levels and two A_2 levels, are part of two weakly coupled components within the network. Their connections to the broader network are limited, leading to less accurate definitions: the Supplementary Material gives details of these states and linked levels. Additionally, the single transition defining the states (2,20, A_2,14) and (2,20, E,28) is given three different assignments in the original source [72]; it is assigned as an F line, an E line, and an A line. We note that F states are generally better defined, as they are characterized by more transitions. More experimental data are required to resolve the above problem and enhance the accuracy of the A and E networks.

4.1. *Magic numbers*

To interconnect previously unlinked networks, including the ortho, para, and meta networks, we use artificial transitions that we call 'magic numbers'. In addition, some extra magic numbers were used. Specifically, the first three (MAGIC.1, MAGIC.2, MAGIC.3) were used to link the ortho, para, and meta networks, the next three (MAGIC.4, MAGIC.5, MAGIC.6) were used to improve the connection between unlinked networks, and the last four (MAGIC.7 to MAGIC.10) connected the first four larger energy components. For this work, the Effective Hamiltonian wavenumber values by 16AmLoPi [72] were utilized as magic numbers, which are listed in Table 2.

4.2. MARVEL *energy uncertainties*

MARVEL calculates energy uncertainties using the input transition uncertainties. In addition to this, when utilized without the bootstrap method, MARVEL yielded an average energy uncertainty of 0.0036 cm^{-1} based purely on the stated input uncertainties. However, when the bootstrap method is applied, the average energy uncertainty increases slightly to 0.0049 cm^{-1} suggesting that the input uncertainties are too low for the cases of polyad 0, 1, and 2. This is shown in Fig. 5 and the mean energy uncertainty per polyad is presented in Table 5.

5. Conclusions and future work

In this paper, we endeavored to compile a thorough database of published experimental methane spectra up to July 2023 which we

Table 3
Experimental data for $^{12}C^{1}H_4$ used in our analysis. Wavelength range and mean line position uncertainty are given in cm^{-1}, A/V: number of available transitions/number of validated transitions, given: an uncertainty is given in the source, CD: an uncertainty is not given in the paper and we used an uncertainty based on combination differences, increased: we increased the uncertainty given in the source. See Section 3.1 for comments on individual sources.

Source	Polyad band	Wavenumber range cm^{-1}	A/V	Mean Unc cm^{-1}	Unc Origin
80ItOz [147]	P_0–P_0	0.00027	1/1	6.00E−13	given
73Curl [148]	P_0–P_0	0.01–0.04	2/2	6.60E−07	given
85Dreizler[a] [70]	P_0–P_0	0.16–0.76	7/7	1.00E−03	CD
85OlAnBa.CH4 [149]	P_0–P_0	0.26–0.51	27/27	2.10E−06	given
73HoGeOz [150]	P_0–P_0	0.3–0.5	3/3	3.30E−06	given
92PuWe [90]	P_0–P_0, P_2–P_2	0.3–0.6	18/18	9.30E−07	given
87OlBaHi [151]	P_1–P_1	0.4–0.6	6/6	1.50E−05	given
73TaUeSh [152]	P_2–P_2	0.5	1/1	3.30E−07	given
75HoGeOz [153]	P_0–P_0	0.6–0.64	3/3	6.60E−06	given
87HiLoCh [154]	P_1–P_1	4–9	14/14	2.80E−06	given
MAGIC[d]	P_0–P_0	10.48–3104.76	10/10	6.00E−03	
17BrCuHi [155]	P_0–P_0, P_1–P_1	37.5–84.5	10/10	8.90E−06	given
10BoPiRo [156]	P_0–P_0, P_1–P_1	59–276.3	193/193	3.00E−03	CD
09AlBaBoBrDyadGs [70]	P_1–P_0	1088.3–1751.8	1189/1182	5.00E−03	increased
16AmLoPi [72]	P_1–P_0, P_2–P_1	1100.4–1488	5062/3846	2.70E−03	given
10SmBePr [157]	P_1–P_0	1159.3–1494.6	435/434	7.20E−04	increased
82JeRo [76]	P_1–P_0	1170.4–1316.9	49/49	1.00E−02	CD
09AlBaBoBrPentDyad [70]	P_2–P_1	1189.3–1930.4	1046/1046	1.00E−03	increased
22GeHjBo [158]	P_1–P_0, P_2–P_1	1250.4–1378.5	712/712	1.90E−02	given
79PiDu [74]	P_1–P_0	1259.5–1306.6	134/128	1.20E−02	increased
98BrKaRu [91]	P_1–P_0, P_2–P_1, P_3–P_2, P_4–P_3	1260–1333.2	295/287	2.00E−03	increased
93HiBaBr [159]	P_2–P_1, P_3–P_2, P_1–P_0	1262.1–1275.5	40/40	1.50E−03	given
79ReCa [160]	P_1–P_0	1292.5–1306.8	89/81	1.00E−02	increased
75ChBe[c] [125]	P_1–P_0	1359.2–1770.2	196/193	6.10E−02	increased
92HiLoBr [161]	P_3–P_0, P_2–P_1	1382.8–4652.2	434/431	7.00E−03	increased
21LiDiLi [162]	P_1–P_0	1396.5–1397.1	10/10	1.00E−03	CD
14SmBePr [163]	P_1–P_0	1398.5–1645	154/150	5.40E−05	given
09AlBaBoBrOctadDyad [70]	P_3–P_1	2334.1–3298.4	1707/1707	2.00E−03	increased
09AlBaBoBrPentadGs [70]	P_2–P_0	2466.5–3274.2	2246/2246	5.00E−03	increased
97MaBeSa[c] [79]	P_4–P_2, P_4–P_0	2868.3–6057.2	76/60	8.70E−03	given
00FeChJoBr [93]	P_2–P_0	2884.3–3149.04	258/257	2.00E−04	given
18KoMaEs [116]	P_2–P_0	2885–3122.8	36/36	1.10E−05	given
13AbIwOk [104]	P_2–P_0	2894.9–3104.6	150/150	1.40E−07	given
11BaGiSw [164]	P_2–P_0	2905.6–3048.2	132/132	9.20E−06	given
92BeSaCa[c] [128]	P_2–P_0	2910.6–2920.7	83/81	1.00E−03	given
76Pine [71]	P_2–P_0	2916.2–3122.8	155/149	5.00E−04	given
79DaPiRo [73]	P_2–P_0	2937.2–3067.3	30/30	5.00E−04	CD
11OkNaIw [165]	P_2–P_0	2943.2–3018.9	54/54	7.70E−08	given
09TaKoSa [166]	P_2–P_0	2947.6–2958.7	12/12	3.60E−07	given
85ChKlNi [80]	P_2–P_0	2947.8–2947.9	3/3	1.50E−07	given
98ErTyKr [92]	P_2–P_0	2947.8	1/1	6.60E−09	given
72EvDaWe [80]	P_2–P_0	2947.9	1/1	1.60E−06	given
76BlEdJo [84]	P_2–P_0	2947.9	1/1	1.40E−06	given
79DoKoTa [80]	P_2–P_0	2947.9	1/1	3.30E−07	given
80ClDaRu [80]	P_2–P_0	2947.9	1/1	4.60E−07	given
80KnEdPe [85]	P_2–P_0	2947.9	1/1	1.00E−07	given
81DoKoTa [80]	P_2–P_0	2947.9	1/1	4.60E−08	given
82ChGoKl [80]	P_2–P_0	2947.9	1/1	1.00E−07	given
92KrLiWe [88]	P_2–P_0	2947.9	1/1	6.60E−09	given
23RiTeJo [167]	P_2–P_0	3009.6–3014.8	12/12	4.70E−04	given
19Pine [168]	P_2–P_0	3012.5–3018.9	66/66	3.90E−05	increased
21OkInOk [123]	P_4–P_2	3017.7–3018.9	10/10	7.10E−08	given
21FoRuSi (pump) [124]	P_2–P_0	3028.75	1/1	5.00E−04	CD
83DeFrPr [77]	P_4–P_2	3034.6–3068.0	4/1	1.00E−01	given
91Jouvard [130]	P_2–P_0	3063.6–3070.2	37/37	1.00E−03	CD
91MiLaSt[c] [129]	P_2–P_0	3063.6–3066.9	13/13	5.70E−04	given
02GrFiTo [169]	P_2–P_0	3182.9–3224.6	100/85	4.20E−04	given
09AlBaBoBrOctadGs [70]	P_3–P_0	3518.8–4746.6	7910/7907	5.00E−03	increased
19RoNiTh [170]	P_3–P_0, P_4–P_1	3760.2–4100	6847/6798	5.00E−03	CD
01HiRoLoTob[b] [171]	P_3–P_0	3797–4099.7	206/205	1.00E−04	CD
01HiRoLoToa [171]	P_3–P_0	3848.6–3871.8	96/90	7.00E−04	given
88Brown [89]	P_3–P_0	3876.7–3890.9	12/10	1.10E−04	given
22RoNiMa [172]	P_3–P_0, P_4–P_1	4100–4300	11341/11304	7.50E−03	CD
05PrBrMa [97]	P_3–P_0	4100.4–4634.9	1432/1401	2.80E−04	increased
17HaPrNi [113]	P_3–P_0	4300–4491.1	59/55	1.00E−04	CD
17HaPrNi(2) [113]	P_3–P_0	4300–4481.1	102/102	6.20E−04	given
20NiRoTh [173]	P_3–P_0, P_4–P_1	4300–4600	9749/9734	9.00E−03	increased
15DeBeSm [174]	P_3–P_0	4499.5–4628.9	307/305	3.90E−04	given
13DaNiTh [175]	P_2–P_0	4600.4–4868.8	1570/1560	1.00E−03	CD
14NiThRe [176]	P_4–P_0	4801.2–5299.9	2725/2715	3.00E−03	CD
13NiBoWe [110]	P_4–P_0	4885.7–6204.6	1194/1170	1.00E−03	given
01RoHiLo [177]	P_4–P_0	4909.4–5271.8	189/184	1.00E−03	CD

(*continued on next page*)

Table 3 (*continued*).

Source	Polyad band	Wavenumber range cm^{-1}	A/V	Mean Unc cm^{-1}	Unc Origin
18MaZhCa [178]	P_4–P_0	4975.8–4984.6	32/32	2.00E−03	increased
17NiThDa [179]	P_4–P_0	300.1–5549.9	2847/2845	1.50E−03	CD
18NiThDa [180]	P_4–P_0, P_5–P_2	5550–5814.3	3467/3446	1.00E−03	CD
10NiLyMi [99]	P_4–P_0	5550.8–6204.6	2550/2549	5.00E−03	given
15NiLyMi [51]	P_4–P_0	5550.8–6204.6	2069/2067	5.00E−03	given
09LyNiPe [181]	P_4–P_0	5556.3–6180.7	452/443	1.00E−03	CD
98GeHeHi [182]	P_4–P_0	5577.4–6076.1	22/15	1.00E−03	CD
18GhMoKa [114]	P_4–P_0	5695.3–5849.9	2079/2049	1.50E−03	given
13CaLeWa [106]	P_4–P_0	5855–6243.4	3436/3414	1.50E−03	CD
13ZoGiBa [111]	P_4–P_0	5870.6–6137.6	348/341	1.20E−03	given
23DuViGa [183]	P_6–P_2, P_7–P_3	5909.9–6215.9	22/19	5.00E−03	CD
21FoRuSi [124]	P_6–P_2	5910.8–6056.5	8/8	1.00E−04	given
21FoRuSiVtype [124]	P_4–P_0	5972–6047	24/24	4.90E−05	given
19YaLiFe [120]	P_4–P_0	6076.1	1/1	1.20E−06	given
16DeMaRe [112]	P_4–P_0	6076.9–6078	12/12	3.80E−05	given
18GoPrKa [115]	P_4–P_0	6076.9–6077.1	6/6	1.80E−07	given
20YaLiPl [122]	P_4–P_0	6076.9–6077.1	6/6	6.30E−05	given
18YaLiFe [118]	P_4–P_0	6077–6077.2	2/2	9.80E−07	given
19LiYaFe [119]	P_4–P_0	6105.6–6107.2	11/11	1.70E−07	given
11NiThRe [184]	P_5–P_0	6256.3–6788.9	717/717	2.40E−03	CD
12CaWaMo [100]	P_5–P_0	6256.3–6788.9	2514/2497	1.50E−03	given
16ReNiCa [109]	P_5–P_0	6294–6780.4	376/376	1.00E−03	CD
16NiReTa [108]	P_5–P_0	6539.4–6799.9	2445/2445	1.00E−03	CD
02HiQu [94]	P_5–P_0	7478.6–7552.9	23/22	1.00E−03	given
05Brown [96]	P_5–P_0	7478.6–7563.9	26/25	1.00E−03	increased
09ScKaGa [98]	P_5–P_0	7478.6–7564	27/26	1.00E−03	CD
12TaQu [95]	P_5–P_0	7509.5–7564	21/21	1.00E−03	given
19NiPrRe [185]	P_6–P_0	8736.2–9159.1	329/329	5.00E−03	increased

[a] Published in [70] from private communication.

[b] Lines assigned by [170].

[c] Raman lines.

[d] Refer to Section 4.1.

used to extract precise empirical rovibrational energy levels. Our primary objective moving forward is to employ this set of energy levels in order to improve the upcoming MM ExoMol line list for methane [56], and generate a high-resolution line list for $^{12}C^{1}H_4$ that can be used for high-resolution exoplanetary and other studies.

The 82173 measured transitions we assembled from 96 articles yielded 23292 energy levels through the MARVEL procedure. With the bootstrap method, 66.8% of MARVEL energy levels have an uncertainty lower than or equal to 0.005 cm^{-1}.

We gathered a plethora of observational unassigned spectra, as well as assigned spectra with a different convention. As mentioned in Section 3.1 we were able to attribute assignments to a large number of such transitions but we still have a large number of experimental sources with transitions that we aim to assign with our final line list. Many of the sources we used successfully also contain a significant number of unassigned lines. In addition, the following sources reported unassigned transitions that we aim to assign as a next step.

12HaBeMi [49] published 324406 unassigned measured lines ranging from 1067 to 3350 cm^{-1} belonging to the dyad, pentad, and octad bands, as well as in hot bands.

85HiLoBr [282] reported 13 $\nu_3 - \nu_4$ assigned lines ranging from 1568 to 1932 cm^{-1} where a different convention is used for the counting numbers.

03NaBe [283] measured methane spectra in the 2000–6400 cm^{-1}, tetradecad, and octad region. They published a number of very accurate lines around 3038 cm^{-1} that can be assigned with our final line list.

82HuLoRo [284] published spectra in the pentad region and in the 2930–3250 cm^{-1} range. Assignments are given for the observed lines without the lower state's counting number.

15HaBeBa [52] reported high-temperature line position measurements and provided 15 lines around 2980 cm^{-1}.

83PiChGu [285] reported 2250–3260 cm^{-1} lines in the pentad region assigned with a different convention for the quantum numbers.

84MaFrPr [286] and **85MaFrPr** [287] reported partly assigned $3\nu_3 - 2\nu_3$ transitions in the range 2940–2995 cm^{-1} and 2890–2935 cm^{-1} respectively.

97Pine [288] reported measured lines in the pentad region and the range 3028–3122 cm^{-1} which are partly assigned, without upper state counting number.

21YoBeDu [289] published partly assigned pentad lines in the range 2750–3200 cm^{-1}.

72HuPoVa [290] reported partly assigned octad transitions in the 4136–4288 cm^{-1} range.

10CaWaKa [291] reported 12865 unassigned measured icosad transitions.

90Margolis [292] reported partly assigned transitions in the tetradecad region and in the range 5597–5635 cm^{-1}.

18GhVaMo [293] reported unassigned tetradecad lines in the 5693–6257 cm^{-1} region.

08KaGaRo [294] published unassigned transitions in the 5850–7700 cm^{-1} region.

12GaChZh [295] reported tetradecad lines in the 6038–6050 cm^{-1} region.

20YaLiPlb [296] reported one very accurate measured line at around 6077 cm^{-1} which was not assigned.

98BoRePl [297] published unassigned 5500–6180 cm^{-1} lines.

13CaLeMo [121] reported unassigned tetradecad lines from 5855 cm^{-1} to 6183 cm^{-1}.

88Margolis [298] reported unassigned or fully assigned transitions in the tetradecad region and the range 5500–6180 cm^{-1}.

09GaKaCa [299] reported $2\nu_3$ unassigned transitions in the 5852–6181 cm^{-1} range.

08FrWaBu [300] reported measured tetradecad lines unassigned or partly assigned in the 5860–6185 cm^{-1} region.

81BrToHu [301] published unassigned lines in the $\nu_2+\nu_3-\nu_2$ band.

22VoKaCa [302] reported lines in the 6015–6115 cm^{-1} region partly assigned.

23OlSiRu [303] measured and partly assigned transitions in the $3\nu_3$, ν_3 bands.

12WaMoKa [304] reported unassigned icosad lines in the 6717–7589 cm^{-1} region.

Table 4
Experimental $^{12}C^{1}H_4$ papers not used in MARVEL analysis.

Source	Wavenumber range cm^{-1}	Comments
48NePlBe [186]	5900–6200	old measurements
52BoThWi [187]	2700–3200	low accuracy
55FeRoWe [188]	1300–1800	old measurements
60RaEaSk [189]	5983–6115	not fully assigned
65MoGaMo [190]		no measurements provided
65Moret [191]		theoretical paper
66HeMoGo [192]		low accuracy
66McDowell [193]		low accuracy
70ClSt[a] [136]		no measurements provided
70HeHuAn [194]	2884–3141	different assignments, low accuracy
70OzYiKh [195]		no lines provided
71HuDa [196]	2884–3141	different assignments, low accuracy
71HuPo [197]	1225–1376	different assignments, low accuracy
72BaSuHu [198]	2884–3139	low accuracy
72Bobin [199]	5891–6107	not fully assigned
72Botineau [75]	1225–1400	not accurate enough
72RoOzKu [200]	100–180	no lines provided
73BeFaCh [201]		no lines provided
73BoFo [202]	2840–3167	no new measurements
73CaDe [203]		not accurate J assignments
73CuOkSm [204]		no new measurements
73DaMa [205]		no lines provided
73Susskind [206]		no new measurements
75Berger [207]	1271–1311	different assignments, low accuracy
75BoHi [208]		different assignments, low accuracy
75Champion [137]	1481–1747	theoretical paper
75RoOz [209]		no new measurements
75TaDaPo [210]	3019–3021	different assignments
76GrRo [126]		no new measurements
76HaBoUe [211]		no new measurements
77AlKoSm [212]		no new measurements
77Berger[a] [140]		different assignments
77Champion [127]		calculated lines
77ToBrHu [213]	2862–3000	different assignments
78BoGu [214]	4157–4425	different assignments, low accuracy
78ChHuSc [215]		no new measurements
78HuBrTo [216]	2700–2862	unassigned lines
78MaHeBy[a] [138]		no lines provided
78OwPaDo[a] [135]	2916–2918	not fully assigned
78OzRo [217]	94–145	not accurate enough
79BlGoLu [218]	1120–1800	not accurate enough
79BoBr [219]		no lines provided
79GrRo [220]		no new measurements
79GrRoPi [221]		not fully assigned
79KoPrSm [132]		no measurements provided
80ChPiBe [141]		no new measurements
80HiDeCh [222]		low accuracy
80Jennings [223]		no measurements provided
80OrRo [224]		no new measurements
80VaEsOw [225]		no measurements provided
81GhHeLo [226]	2832–3018	not accurate enough
81HuBrTo [227]		difficult to scan table
81OzGeRo [228]	0.00026–0.64	no new measurements
81Robiette [229]		no new measurements
81ToBrHu [230]	2385–3200	no lines provided
82BrRo [231]		no new measurements
82BrToRo [232]	2700–3000	difficult to scan
82LoBrRo [144]	2460–2675	different assignments
82LuPiPiCh [233]		no line position measurements
82RaCa [234]		no new measurements
82PoPaCh [235]	2250–3250	observed energy levels
83BrMaNo [236]		no new measurements
83FrIlFi[a] [142]	2916–2917	different assignments
83VaGiVa.a [237]		unassigned lines
85BrTo [238]		no line position measurements
85GrLa [133]		no lines provided
85ThFaKo[a] [134]		not accurate enough
86KeCoSm [239]		no new measurements
87Kim [240]		intensity measurements
86TyChPi [241]		no new measurements
89BrLoHi [242]		no new measurements
89VaCh [243]	1270–1317	not fully assigned
90VaCh [244]	1332–1350	no new measurements

(*continued on next page*)

Table 4 (*continued*).

Source	Wavenumber range cm^{-1}	Comments
91RoCh [245]		no new measurements
92BrMaCh [246]		no new measurements
92Pine [247]	3012–3018	we used the lines from [168]
92SaCaDo[a] [131]	2916–2917	no new measurements
92SmRiDe [248]		no new measurements
96OuHiLo [249]		no new measurements
98WeCh [250]		theoretical paper
00MeDoMe [251]	2942–2982	not fully assigned
01NaMi [252]	3009–3039	not fully assigned
02BrCa [253]	10635–13300	no lines provided
05GhBu [254]		no new line measurements
05JoChSa [143]	1200–5500	no lines provided
05MoChVa [255]	2914–2922	no new line measurements
06BoMeMa [256]	2931–2996	no new line measurements
06BoReLo [69]		theoretical paper
07JoGaCh[a] [145]	2905–2925	no lines provided
07RuWoHa [257]	2990–3070	not fully assigned
07WiOrOz [258]	0.06–0.24	no lines provided
10HoSkSa [259]		not fully assigned
10TrHaTo [260]	6000	no new line measurements
10ZiWh [261]		theoretical paper
12SaAuPi [262]	59–288	no new line measurements
12YuFaYa [263]		no new line measurements
13ThDaAn [3]		no new line measurements
13TyTaRe [117]		theoretical paper
14ReNiTY [264]		theoretical paper
14UlBeAl [67]	1000–12500	no lines provided
15LiWaTa [265]		no new line measurements
15MaKcVa[a] [139]	882–3434	unassigned
15ReNiTy [103]		theoretical paper
17ReNiTy [53]		theoretical paper
18NiPrRe [266]		theoretical paper
18Petrov [267]		no new line measurements
18ReNiBe [268]	0–3400	theoretical paper
19BuAmBe [269]		no lines provided
19DeGhHo [270]		no new line measurements
19GhHeBe [271]		no new line measurements
19KiMaPe [272]		no new line measurements
20GiNaTu [273]		no new line measurements
20HaGoRe [55]		theoretical paper
20PeMaZa [274]		theoretical paper
21CuHiMo [275]		no new line measurements
21FaArVa [276]		no new line measurements
21FoRuSib [277]	3028–6058	no new data
21EsFa [278]	2884–2969	no new line measurements
22ZhXuWa [279]	3225.8–3857.1	no lines provided
23MaThCa [280]		no lines provided
23VaDeKa [281]		no new line measurements

[a] Raman lines.

Table 5
Summary of the MARVEL energies. MU/MUb: The Mean Energy Uncertainty before (MU) and after bootstrap (MUb).

Polyad	Energy range cm^{-1}	Number of energy levels	Max J	MU/MUb.
P_0	0–3628.25	247	26	0.005/0.01
P_1	1310.7–5054.83	1088	27	0.005/0.01
P_2	2587.04–6239.03	3154	27	0.005/0.009
P_3	3870.48–7017.60	7708	23	0.005/0.006
P_4	5121.72–7417.90	8232	18	0.002/0.002
P_5	6377.52–7903.64	2528	15	0.001/0.001
P_6	8562.46–9629.88	333	10	0.005/0.005
P_7	9832.06–9986.23	2	4	0.005/0.005

21MaYuSu [305] reported unassigned icosad lines in the 6770–7570 cm^{-1} region.

09ScKaGa [98] reported unassigned icosad lines in the 7351–7655 cm^{-1} region.

05Brown [96] published observed lines in the range 6770 to 9111 cm^{-1}.

19WoBeRe [306] published 5200–9200 cm^{-1} unassigned lines belonging to the tetradecad, icosad, and triacodad regions.

13MaPrMo [307] reported 654 icosad transitions in the range 7040–7378 cm^{-1} partly assigned or unassigned.

11MoKaWa [308] published unassigned spectra in the 7541–7919 cm^{-1} range.

19WoBeRe [306] reported unassigned measured transitions in the tetradecad, icosad, and triacodad and in the range 5200–9200 cm^{-1}.

96SiOb [309] provided unassigned spectra from 7128 to 7373 cm^{-1}.

15BeKaCa [310] reported unassigned measured spectra in the range 7908–8345 cm^{-1}.

80PiHiBe [311] reported partly assigned $3\nu_3$ lines in the range 9000–9155 cm^{-1}.

18SeSiLu [312] reported unassigned 9057-9167 cm^{-1} lines.

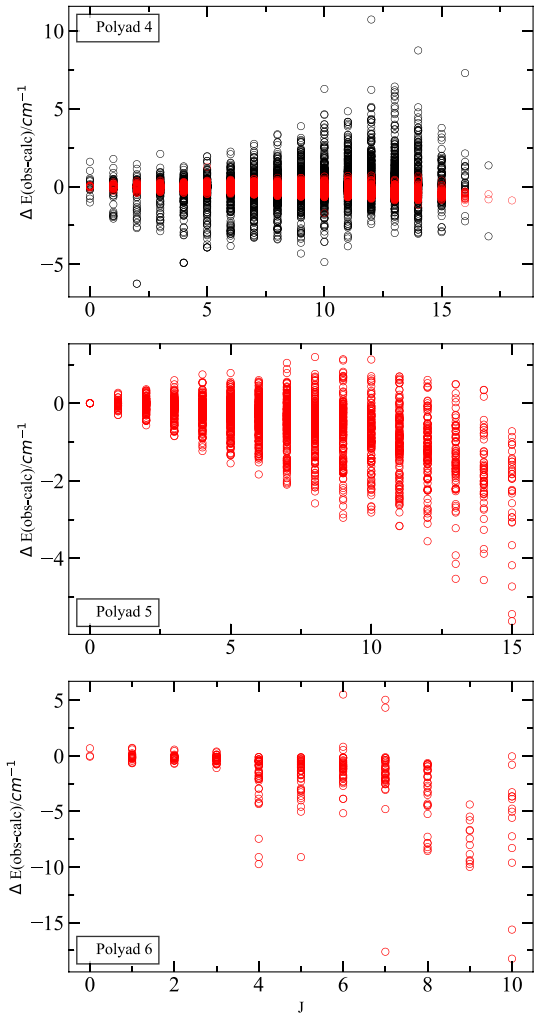

Fig. 4. Difference between the MARVEL energies (obs) and the a. Effective Hamiltonian by [72] (black) b. Variational calculations (red) by [53].

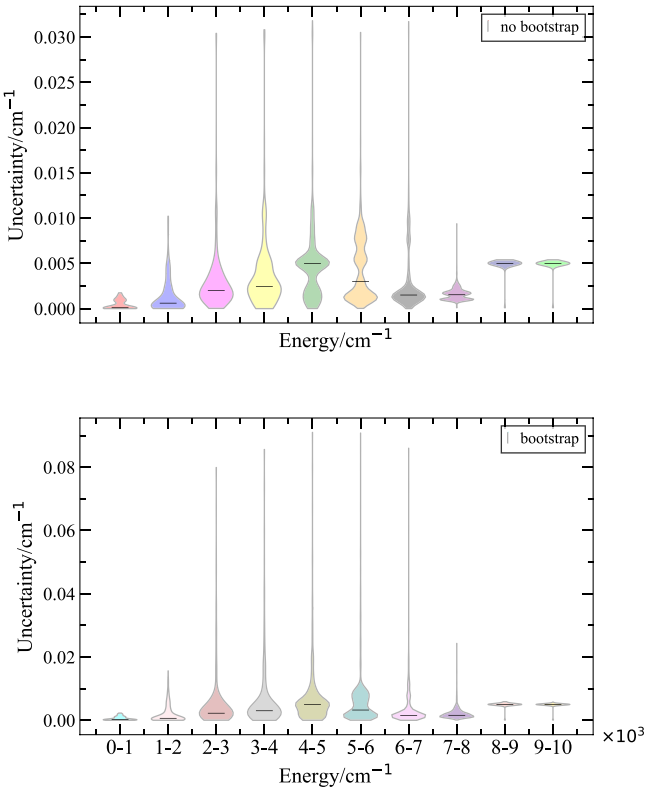

Fig. 5. The MARVEL energy uncertainties with respect to the energy.

15BeLiCa [313] reported triacodad transitions in the 9028–10435 cm^{-1} region.

93BoBoLi [314] reported three partly assigned measured lines in the range 11258–11309 cm^{-1}.

07LuGo [315] reported observed transitions at around 11900 cm^{-1} belonging to the $\nu_1 + 3\nu_3$ band.

95TsSa [316] reported $3\nu_1 + \nu_3$ unassigned lines.

94BoLiRe [317] published $3\nu_1 + \nu_3$ transitions in the range 11220–11313 cm^{-1} mostly unassigned.

95CaPeJo [318] published partly assigned transitions in the range 11245–11312 cm^{-1}.

93LuLoGa [319] measured unassigned lines in the 11539–12756 cm^{-1} region.

22Lucchesini [320] reported 112 unassigned lines in the heptacontad region at around 12700 cm^{-1}.

95SiOb [321] reported 13470–14025 cm^{-1} unassigned lines.

91CaChSt [322] reported $4\nu_1 + \nu_3$ lines in the range 13702–13887 cm^{-1}.

Finally, we note that **23CaKaVaTu** [323] very recently published an unassigned absorption spectrum in the range 10800–14000 cm^{-1}.

CRediT authorship contribution statement

Kyriaki Kefala: Writing – original draft, Validation, Formal analysis, Data curation. **Vincent Boudon:** Methodology, Formal analysis. **Sergei N. Yurchenko:** Writing – review & editing, Validation, Methodology. **Jonathan Tennyson:** Writing – review & editing, Supervision, Funding acquisition, Conceptualization.

Declaration of competing interest

The authors declare no competing financial interests.

Data availability

All data given in the supporting material.

Acknowledgments

We would like to thank Tibor Furtenbacher for his constant support during the process, by addressing issues and questions related to MARVEL. In addition, we thank Michael Rey and Robert Gamache for providing us with a variationally calculated methane line list by TheoReTS, and Emma Barton and her ORBYTS team for initial work on this project. This work was funded by the European Research Council (ERC) under the European Union's Horizon 2020 research and innovation programme through Advance Grant number 883830 and STFC, UK through grant ST/R000476/1.

Appendix A. Supplementary material

The MARVEL transition, energy, and segment files are provided as supplementary material as well an analysis of the outlying levels discussed in Section 4.

Supplementary material related to this article can be found online at https://doi.org/10.1016/j.jqsrt.2024.108897.

References

[1] Maslin M, Owen M, Betts R, Day S, Dunkley Jones T, Ridgwell A. Gas hydrates: past and future geohazard? Phil Trans R Soc A 2010;368(1919):2369–93. http://dx.doi.org/10.1098/rsta.2010.0065.

[2] Heimann M. Enigma of the recent methane budget. Nature 2011;476:157–8.

[3] Thomas B, David G, Anselmo C, Coillet E, Rieth K, Miffre A, et al. Remote sensing of methane with broadband laser and optical correlation spectroscopy on the Q-branch of the $2\nu_3$ band. J Mol Spectrosc 2013;291:3–8. http://dx.doi.org/10.1016/j.jms.2013.05.015.

[4] Houghton J. Global warming. Rep Progr Phys 2005;68:1343. http://dx.doi.org/10.1088/0034-4885/68/6/R02.

[5] Rhoderick GC, Dorko WD. Standards development of global warming gas species: Methane, nitrous oxide, trichlorofluoromethane, and dichlorodifluoromethane. Environ Sci Technol 2004;38:2685–92. http://dx.doi.org/10.1021/es035424i.

[6] Staniaszek Z, Griffiths PT, Folberth GA, O'Connor FM, Abraham NL, Archibald AT. The role of future anthropogenic methane emissions in air quality and climate. NPJ Clim Atmospheric Sci 2022;5:21.

[7] Van Amstel A. Methane. A review. J Integr Environ Sci 2012;9:5–30. http://dx.doi.org/10.1080/1943815X.2012.694892.

[8] Guzmán-Marmolejo A, Segura A. Methane in the solar system. Boletín de la Sociedad Geológica Mexicana 2015;67:377–85.

[9] Taylor FW, Atreya SK, Encrenaz T, Hunten DM, Irwin PGJ, Owen TC. The composition of the atmosphere of jupiter, Jupiter: the planet, satellites and magnetosphere. 2004, p. 59–78.

[10] Fletcher LN, Orton GS, Teanby NA, Irwin PGJ, Bjoraker GL. Methane and its isotopologues on Saturn from Cassini/CIRS observations. Icarus 2009;199:351–67. http://dx.doi.org/10.1016/j.Icarus.2008.09.019.

[11] Teifel VG. Methane abundance in the atmosphere of Uranus. Icarus 1983;53:389–98.

[12] Baines KH, Mickelson ME, Larson LE, Ferguson DW. The abundances of methane and ortho/para hydrogen on uranus and neptune: Implications of new laboratory 4-0 H_2 quadrupole line parameters. Icarus 1995;114:328–40. http://dx.doi.org/10.1006/icar.1995.1065.

[13] Oyama VI, Carle GC, Woeller F, Pollack JB, Reynolds RT, Craig RA. Pioneer Venus gas chromatography of the lower atmosphere of Venus. J Geophys Res: Space 1980;85:7891–902. http://dx.doi.org/10.1029/JA085iA13p07891.

[14] Niemann HB, Atreya SK, Bauer SJ, Carignan GR, Demick JE, Frost RL, et al. The abundances of constituents of Titan's atmosphere from the GCMS instrument on the Huygens probe. Nature 2005;438:779–84. http://dx.doi.org/10.1038/nature04122.

[15] Waite JH, Niemann H, Yelle RV, Kasprzak WT, Cravens TE, Luhmann JG, et al. Ion neutral mass spectrometer results from the first flyby of Titan. Science 2005;308:982–6. http://dx.doi.org/10.1126/science.1110652.

[16] Boudon V, Champion J-P, Gabard T, Loëte M, Coustenis A, De Bergh C, et al. Methane in Titan's atmosphere: from fundamental spectroscopy to planetology. Europhys News 2009;40:17–20.

[17] Lellouch E, de Bergh C, Sicardy B, Ferron S, Käufl H-U. Detection of CO in Triton's atmosphere and the nature of surface-atmosphere interactions. Astron Astrophys 2010;512:L8.

[18] Grundy WM, Young LA. Near-infrared spectral monitoring of Triton with IRTF/SpeX I: establishing a baseline for rotational variability. Icarus 2004;172:455–65. http://dx.doi.org/10.1016/j.icarus.2004.07.013.

[19] Cruikshank DP, Apt J. Methane on Triton: Physical state and distribution. Icarus 1984;58:306–11. http://dx.doi.org/10.1016/0019-1035(84)90047-2.

[20] Merlin F, Lellouch E, Quirico E, Schmitt B. Triton's surface ices: Distribution, temperature and mixing state from VLT/SINFONI observations. Icarus 2018;314:274–93. http://dx.doi.org/10.1016/j.icarus.2018.06.003.

[21] Krasnopolsky VA, Maillard JP, Owen TC. Detection of methane in the martian atmosphere: evidence for life? Icarus 2004;172:537–47. http://dx.doi.org/10.1016/j.Icarus.2004.07.004.

[22] Giuranna M, Viscardy S, Daerden F, Neary L, Etiope G, Oehler D, et al. Independent confirmation of a methane spike on Mars and a source region east of Gale Crater. Nat Geosci 2019;12:326–32.

[23] Grenfell JL, Wunderlich F, Sinnhuber M, Herbst K, Lehmann R, Scheucher M, et al. Atmospheric processes affecting methane on Mars. Icarus 2022;382:114940. http://dx.doi.org/10.1016/j.Icarus.2022.114940.

[24] Webster CR, Mahaffy PR, Atreya SK, Flesch GJ, Farley KA. MSL Science Team, Low upper limit to methane abundance on Mars. Science 2013;342:355–7. http://dx.doi.org/10.1126/science.1242902.

[25] Zahnle K, Freedman RS, Catling DC. Is there methane on Mars? Icarus 2011;212:493–503. http://dx.doi.org/10.1016/j.icarus.2010.11.027.

[26] Korablev O, Vandaele AC, Montmessin F, Fedorova AA, Trokhimovskiy A, Forget F, et al. No detection of methane on Mars from early ExoMars Trace Gas Orbiter observations. Nature 2019;568(7753):517–20.

[27] Krasnopolsky VA. Some problems related to the origin of methane on Mars. Icarus 2006;180:359–67.

[28] Allen M, Delitsky M, Huntress W, Yung Y, Ip WH. Evidence for methane and ammonia in the coma of comet P/Halley. Astron Astrophys 1987;187:502–12.

[29] Gibb EL, Mumma MJ, Dello Russo N, DiSanti MA, Magee-Sauer K. Methane in Oort cloud comets. Icarus 2003;165:391–406. http://dx.doi.org/10.1016/S0019-1035(03)00201-X.

[30] Apt J, Carleton NP, MacKay CD. Methane on Triton and Pluto - new CCD spectra. Astrophys J 1983;270:342–50. http://dx.doi.org/10.1086/161127.

[31] Oppenheimer BR, Kulkarni SR, Matthews K, Nakajima T. Infrared Spectrum of the Cool Brown Dwarf Gl 229B. Science 1995;270:1478–9. http://dx.doi.org/10.1126/science.270.5241.1478.

[32] Bernath PF. Molecular astronomy of cool stars and sub-stellar objects. Intern Rev Phys Chem 2009;28:681–709.

[33] Hauschildt PH, Warmbier R, Schneider R, Barman T. Methane line opacities in very cool stellar objects. Astron Astrophys 2009;504:225–9. http://dx.doi.org/10.1051/0004-6361/200912366.

[34] Swain MR, Vasisht G, Tinetti G. The presence of methane in the atmosphere of an extrasolar planet. Nature 2008;452:329–31. http://dx.doi.org/10.1038/Nature06823.

[35] Sagan C, Thompson WR, Carlson R, Gurnett D, Hord C. A search for life on earth from the Galileo spacecraft. Nature 1993;365:715–21. http://dx.doi.org/10.1038/365715a0.

[36] Schindler TL, Kasting JF. Synthetic spectra of simulated terrestrial atmospheres containing possible biomarker gases. Icarus 2000;145:262–71.

[37] Thompson MA, Krissansen-Totton J, Wogan N, Telus M, Fortney JJ. The case and context for atmospheric methane as an exoplanet biosignature. Proc Natl Acad Sci 2022;119:e2117933119. http://dx.doi.org/10.1073/pnas.2117933119.

[38] Öberg KI, Murray-Clay R, Bergin EA. The effects of snowlines on C/O in planetary atmospheres. Astrophys J 2011;743:L16. http://dx.doi.org/10.1088/2041-8205/743/1/L16.

[39] Swain MR, Deroo P, Griffith CA, Tinetti G, Thatte A, Vasisht G, et al. A ground-based near-infrared emission spectrum of the exoplanet HD 189733b. Nature 2010;463:637–9.

[40] Swain MR, Tinetti G, Vasisht G, Deroo P, Griffith C, Bouwman J, et al. Water, methane, and carbon dioxide present in the dayside spectrum of the exoplanet HD 209458b. Astrophys J 2009;704:1616.

[41] Tinetti G, Deroo P, Swain MR, Griffith CA, Vasisht G, Brown LR, et al. Probing the terminator region atmosphere of the hot-Jupiter XO-1b with transmission spectroscopy. Astrophys J Lett 2010;712:L139.

[42] Stevenson KB, Harrington J, Nymeyer S, Madhusudhan N, Seager S, Bowman WC, et al. Possible thermochemical disequilibrium in the atmosphere of the exoplanet GJ 436b. Nature 2010;464:1161–4.

[43] Beaulieu JP, Tinetti G, Kipping D, Ribas I, Barber RJ, Cho JY-K, et al. Methane in the atmosphere of the transiting hot Neptune GJ436b? Astrophys J 2011;731:16.

[44] Fukui A, Narita N, Kurosaki K, Ikoma M, Yanagisawa K, Kuroda D, et al. Optical-to-near-infrared simultaneous observations for the hot Uranus GJ3470b: a hint of a cloud-free atmosphere. Astrophys J 2013;770:95. http://dx.doi.org/10.1088/0004-637X/770/2/95.

[45] Venot O, Agúndez M, Selsis F, Tessenyi M, Iro N. The atmospheric chemistry of the warm Neptune GJ 3470b: Influence of metallicity and temperature on the CH_4/CO ratio. Astron Astrophys 2014;562:A51.

[46] Guilluy G, Sozzetti A, Brogi M, Bonomo AS, Giacobbe P, Claudi R, et al. Exoplanet atmospheres with GIANO-II. Detection of molecular absorption in the dayside spectrum of HD 102195b. Astron Astrophys 2019;625:A107.

[47] Showman AP. A whiff of methane. Nature 2008;452:296–7.

[48] Borysow A, Champion JP, Jorgensen UG, Wenger C. Preliminary CH_4 line list data for stellar atmospheres. In: Hubeny I, Mihalas D, Werner K, editors. Stellar atmosphere modeling. ASP conference series, vol. 288, 2003, p. 352–6.

[49] Hargreaves RJ, Beale CA, Michaux L, Irfan M, Bernath PF. Hot methane line lists for exoplanet and brown dwarf atmospheres. Astrophys J 2012;757:46. http://dx.doi.org/10.1088/0004-637X/757/1/46.

[50] Yurchenko SN, Tennyson J. ExoMol line lists IV: The rotation-vibration spectrum of methane up to 1500 K. Mon Not R Astron Soc 2014;440:1649–61. http://dx.doi.org/10.1093/mnras/stu326.

[51] Nikitin A, Lyulin O, Mikhailenko S, Perevalov V, Filippov N, Grigoriev I, et al. Gosat-2014 methane spectral line list. J Quant Spectrosc Radiat Transf 2014;154(2015):63–71. http://dx.doi.org/10.1016/j.jqsrt.2014.12.003, https://www.sciencedirect.com/science/article/pii/S0022407314004750.

[52] Hargreaves RJ, Bernath PF, Bailey J, Dulick M. Empirical line lists and absorption cross sections for methane at high temperatures. Astrophys J 2015;813:12. http://dx.doi.org/10.1088/0004-637X/813/1/12.

[53] Rey M, Nikitin AV, Tyuterev VG. Accurate theoretical methane line lists in the infrared up to 3000 K and quasi-continuum absorption/emission modeling for astrophysical applications. Astrophys J 2017;847:105. http://dx.doi.org/10.3847/1538-4357/aa8909.

[54] Makhnev VY, Kyuberis AA, Zobov NF, Lodi L, Tennyson J, Polyansky OL. High accuracy ab initio calculations of rotation-vibration energy levels of the HCN/HNC system. J Phys Chem A 2018;122:1326–43. http://dx.doi.org/10.1021/acs.jpca.7b10483.

[55] Hargreaves RJ, Gordon IE, Rey M, Nikitin AV, Tyuterev VG, Kochanov RV, et al. An accurate, extensive, and practical line list of methane for the HITEMP database. Astrophys J Suppl 2020;247:55. http://dx.doi.org/10.3847/1538-4365/ab7a1a.

[56] Yurchenko SN, Owens A, Kefala K, Tennyson J. ExoMol line lists – LVII. High accuracy ro-vibrational line list for methane (CH_4). Mon Not R Astron Soc.

[57] Yurchenko SN, Thiel W, Jensen P. Theoretical ROVibrational Energies (TROVE): A robust numerical approach to the calculation of rovibrational energies for polyatomic molecules. J Mol Spectrosc 2007;245:126–40. http://dx.doi.org/10.1016/j.jms.2007.07.009.

[58] Furtenbacher T, Csaszar AG, Tennyson J. MARVEL: measured active rotational-vibrational energy levels. J Mol Spectrosc 2007;245:115–25. http://dx.doi.org/10.1016/j.jms.2007.07.005.

[59] Furtenbacher T, Császár AG. MARVEL: measured active rotational-vibrational energy levels, II. Algorithmic improvements. J Quant Spectrosc Radiat Transf 2012;113:929–35. http://dx.doi.org/10.1016/j.jqsrt.2012.01.005.

[60] Furtenbacher T, Császár AG. The role of intensities in determining characteristics of spectroscopic networks. J Mol Struct 2012;1009:123–9. http://dx.doi.org/10.1016/j.molstruc.2011.10.057.

[61] Tóbiás R, Furtenbacher T, Tennyson J, Császár AG. Accurate empirical rovibrational energies and transitions of $H_2^{16}O$. Phys Chem Chem Phys 2019;21:3473–95. http://dx.doi.org/10.1039/c8cp05169k.

[62] Császár AG, Furtenbacher T. Spectroscopic networks. J Mol Spectrosc 2011;266:99–103. http://dx.doi.org/10.1016/j.jms.2011.03.031.

[63] Császár AG, Czakó G, Furtenbacher T, Mátyus E. An active database approach to complete rotational–vibrational spectra of small molecules. Annu Rep Comput Chem 2007;3:155–76.

[64] Furtenbacher T, Árendás P, Mellau G, Császár AG. Simple molecules as complex systems. Sci Rep 2014;4:4654.

[65] Tennyson J, Furtenbacher T, Yurchenko SN, Császár AG. Empirical rovibrational energy levels for nitrous oxide. J Quant Spectrosc Radiat Transf.

[66] Bunker P, Jensen P. Fundamentals of molecular symmetry. IOP Publishing; 2004, http://dx.doi.org/10.1201/9781315273334.

[67] Ulenikov ON, Bekhtereva ES, Albert S, Bauerecker S, Niederer HM, Quack M. Survey of the high resolution infrared spectrum of methane ($^{12}CH_4$ and $^{13}CH_4$): Partial vibrational assignment extended towards 12 000 cm^{-1}. J Chem Phys 2014;141:234302. http://dx.doi.org/10.1063/1.4899263.

[68] Champion J-P, Loëte M, Pierre G. Spherical top spectra. In: Narahari Rao K, Weber A, editors. Spectroscopy of the earth's atmosphere and interstellar medium. USA: Academic Press, Inc; 1992, p. 339–422.

[69] Boudon V, Rey M, Loete M. The vibrational levels of methane obtained from analyses of high-resolution spectra. J Quant Spectrosc Radiat Transfer 2006;98:394–404. http://dx.doi.org/10.1016/j.jqsrt.2005.06.003.

[70] Albert S, Bauerecker S, Boudon V, Brown LR, Champion J-P, Loëte M, et al. Global analysis of the high resolution infrared spectrum of methane $^{12}CH_4$ in the region from 0 to 4800 cm^{-1}. Chem Phys 2009;356:131–46.

[71] Pine AS. High-resolution methane ν_3-band spectra using a stabilized tunable difference-frequency laser system. J Opt Soc Amer 1976;66:97–108. http://dx.doi.org/10.1364/JOSA.66.000097.

[72] Amyay B, Louviot M, Pirali O, Georges R, Vander Auwera J, Boudon V. Global analysis of the high temperature infrared emission spectrum of $^{12}CH_4$ in the dyad (ν_2/ν_4) region. J Chem Phys 2016;144:024312. http://dx.doi.org/10.1063/1.4939521.

[73] Dang-Nhu M, Pine AS, Robiette AG. Spectral Intensities in the ν_3 Bands of $^{12}CH_4$ and $^{13}CH_4$. J Mol Spectrosc 1979;77:57–68.

[74] Pinson P, Dupre-Maquaire J. The high resolution spectrum of CH_4: The Q branch of the ν_4 band. J Mol Spectrosc 1979;78:170–4.

[75] Botineau J. Infrared-absorption of methane at high-resolution between 1225 and 1400 cm^{-1}. J Mol Spectrosc 1972;41:182. http://dx.doi.org/10.1016/0022-2852(72)90131-2.

[76] Jennings DE, Robiette AG. Determination of the ν_4 band strength of $^{12}CH_4$ from diode-laser line strength measurements. J Mol Spectrosc 1982;94:369–79. http://dx.doi.org/10.1016/0022-2852(82)90013-3.

[77] De Martino A, Frey R, Pradere F. Double-resonance observation of the ($2\nu_3$, E) state in methane. Chem Phys Lett 1983;95:200–4.

[78] De Martino A, Frey R, Pradere F. Observation of the $\nu_3 - (2\nu_3, A_1)$ band of methane. Chem Phys Lett 1983;100:329–33.

[79] Martinez RZ, Bermejo D, Santos J, Champion JP, Hilico JC. High resolution Raman spectroscopy from vibrationally excited states populated by a stimulated Raman process: $2\nu_1 - \nu_1$ of $^{12}CH_4$. J Chem Phys 1997;107:4864–74.

[80] Chebotayev VP, Klementyev VM, Nikitin MV, Timchenko BA, Zakharyash VF. Comparison of frequency stabilities of the Rb standard and of the He-Ne/CH_4 laser stabilized to the E-line in methane. Appl Phys B Photophys Laser Chem 1985;36:59–61. http://dx.doi.org/10.1007/BF00698038.

[81] Domnin YS, Koshelyayevsky MB, Tatarenkov VM, Shumyatsky PS. Absolute measurements of frequencies of IR lasers (rus). JETP Lett 1979;30:273.

[82] Domnin YS, Koshelyayevsky MB, Tatarenkov VM, Shumyatsky PS. He-Ne/CH4 laser frequency measurements (rus). JETP Lett 1981;34:175.

[83] Chebotayev VP, Goldort VG, Klementyev VM, Nikitin MV, Timchenko BA, Zakharyash VF. Development of an optical-time scale. Appl Phys B Photophys Laser Chem 1982;29:63–5. http://dx.doi.org/10.1007/BF00694370.

[84] Blaney TG, Edwards GJ, Jolliffe BW, Knight DJE, Woods PT. Absolute frequencies of the methane-stabilized HeNe laser (3.39μm) and the CO_2, R(32) stabilized laser (10.17μm). J Phys D: Appl Phys 1976;9:1323. http://dx.doi.org/10.1088/0022-3727/9/9/009.

[85] Knight DJE, Edwards GJ, Pearce PR, Cross NR. Measurement of the frequency of the 3.39-μm methane-stabilized laser to ±3 parts in 10^{-11}. IEEE Trans Instrum Meas 1980;29:257–64. http://dx.doi.org/10.1109/TIM.1980.4314930.

[86] Clairon A, Dahmani B, Rutman J. Accurate absolute frequency measurements on stabilized CO_2 and He-Ne infrared-lasers. IEEE Trans Instrum Meas 1980;29:268–72. http://dx.doi.org/10.1109/TIM.1980.4314932.

[87] Evenson KM, Day GW, Wells JS, Mullen LO. Extension of absolute frequency measurements to the cw He–Ne Laser at 88 THz (3.39 μ). Appl Phys Lett 1972;20:133–4.

[88] Kramer G, Lipphardt B, Weiss CO. Coherent frequency-synthesis in the infrared. In: Proceedings of the 1992 IEEE frequency control symposium. IEEE, Ultrasonics, Ferroelectrics, and Frequency Control Society; 1992, p. 39–43.

[89] Brown LR. Methane line parameters from 3700 to 4136 cm^{-1}. Appl Opt 1988;27:3275–9.

[90] Pursell CJ, Weliky DP. Pure rotational transitions in the ν_3 state of methane. J Mol Spectrosc 1992;97:773–85.

[91] Bronnikov DK, Kalinin DV, Rusanov VD, Filimonov YG, Selivanov YG, Hilico JC. Spectroscopy and non-equilibrium distribution of vibrationally excited methane in a supersonic jet. J Quant Spectrosc Radiat Transfer 1998;60:1053–68.

[92] Ering PS, Tyurikov DA, Kramer G, Lipphardt B. Measurement of the absolute frequency of the methane E-line at 88 THz. Opt Comms 1998;151:229–34.

[93] Fejard L, Champion JP, Brown LR, Pine AS. The intensities of methane in the 3 to 5μm region revisited. J Mol Spectrosc 2000;201:83–94.

[94] Hippler M, Quack M. High-resolution Fourier transform infrared and cw-diode laser cavity ringdown spectroscopy of the ν_2+2 nu(3) band of methane near 7510 cm^{-1} in slit jet expansions and at room temperature. J Chem Phys 2002;116:6045–55. http://dx.doi.org/10.1063/1.1433505.

[95] Tanner CM, Quack M. Reinvestigation of the $\nu_2 + 2\nu_3$ subband in the overtone icosad of $^{12}CH_4$ using cavity ring-down (CRD) spectroscopy of a supersonic jet expansion. Mol Phys 2012;110(17, SI):2111–35. http://dx.doi.org/10.1080/00268976.2012.702934.

[96] Brown LR. Empirical line parameters of methane from 1.1 to 2.1μm. J Quant Spectrosc Radiat Transfer 2005;96:251–70. http://dx.doi.org/10.1016/j.jqsrt.2004.12.037.

[97] Predoi-Cross A, Brown LR, Malathy-Devi V, Brawley-Tremblay M, Benner D. Multispectrum analysis of $^{12}CH_4$ from 4100 to 4635 cm^{-1}: 1, self-broadening coefficients (widths and shifts). J Mol Spectrosc 2005;232:231–46.

[98] Sciamma-O'Brien E, Kassi S, Gao B, Campargue A. Experimental low energy values of CH_4 transitions near 1.33μm by absorption spectroscopy at 81 K. J Quant Spectrosc Radiat Transfer 2009;110:951–63. http://dx.doi.org/10.1016/j.jqsrt.2009.02.004.

[99] Nikitin AV, Lyulin OM, Mikhailenko SN, Perevalov VI, Filippov NN, Grigoriev IM, et al. GOSAT-2009 methane spectral line list in the 5550-6236 cm^{-1} range. J Quant Spectrosc Radiat Transf 2009;111(2010):2211–24. http://dx.doi.org/10.1016/j.jqsrt.2010.05.010.

[100] Campargue A, Wang L, Mondelain D, Kassi S, Bezard B, Lellouch E, et al. An empirical line list for methane in the 1.26-1.71μm region for planetary investigations (T=80-300 K). Application to Titan. Icarus 2012;219:110–28. http://dx.doi.org/10.1016/j.Icarus.2012.02.015.

[101] Rothman LS, et al. The HITRAN 2012 molecular spectroscopic database. J Quant Spectrosc Radiat Transf 2012;130(2013):4–50. http://dx.doi.org/10.1016/jqsrt.2013.07.002.

[102] Gordon IE, et al. The HITRAN2020 molecular spectroscopic database. J Quant Spectrosc Radiat Transf 2020;277(2022):107949. http://dx.doi.org/10.1016/j.jqsrt.2021.107949.

[103] Rey M, Nikitin AV, Tyuterev VG. Convergence of normal mode variational calculations of methane spectra: Theoretical linelist in the icosad range computed from potential energy and dipole moment surfaces. J Quant Spectrosc Radiat Transfer 2015;164:207–20. http://dx.doi.org/10.1016/j.jqsrt.2015.06.009.

[104] Abe M, Iwakuni K, Okubo S, Sasada H. Accurate transition frequency list of the ν_3 band of methane from sub-Doppler resolution comb-referenced spectroscopy. J Opt Soc Amer B 2013;30:1027–35. http://dx.doi.org/10.1364/JOSAB.30.001027.

[105] Amyay B, Boudon V. Vibration–rotation energy levels and corresponding eigenfunctions of $^{12}CH_4$ up to the tetradecad. J Quant Spectrosc Radiat Transfer 2018;219:85–104. http://dx.doi.org/10.1016/j.jqsrt.2018.08.002.

[106] Campargue A, Leshchishina O, Wang L, Mondelain D, Kassi S. The WKLMC empirical line lists (5852-7919 cm^{-1}) for methane between 80 K and 296 K: Final lists for atmospheric and planetary applications. J Mol Spectrosc 2013;291:16–22. http://dx.doi.org/10.1016/j.jms.2013.03.001.

[107] Nikitin AV, Chizhmakova IS, Rey M, Tashkun SA, Kassi S, Mondelain D, et al. Analysis of the absorption spectrum of $^{12}CH_4$CH4 in the region 5855-6250 cm^{-1} of the $2\nu_3$ band. J Quant Spectrosc Radiat Transfer 2017;203:341–8. http://dx.doi.org/10.1016/j.jqsrt.2017.05.014.

[108] Nikitin AV, Rey M, Tashkun SA, Kassi S, Mondelain D, Campargue A, et al. Analyses and modeling of the $^{12}CH_4$ spectrum at 80 K between 6539 and 6800 cm^{-1}. J Quant Spectrosc Radiat Transfer 2016;168:207–16. http://dx.doi.org/10.1016/j.jqsrt.2015.09.014.

[109] Rey M, Nikitin AV, Campargue A, Kassi S, Mondelain D, Tyuterev VG. Ab initio variational predictions for understanding highly congested spectra: rovibrational assignment of 108 new methane sub-bands in the icosad range (6280-7800 cm^{-1}). Phys Chem Chem Phys 2016;18:176–89. http://dx.doi.org/10.1039/c5cp05265c.

[110] Nikitin AV, Boudon V, Wenger C, Albert S, Brown LR, Bauerecker S, et al. High resolution spectroscopy and the first global analysis of the Tetradecad region of methane $^{12}CH_4$. Phys Chem Chem Phys 2013;15:10071–93. http://dx.doi.org/10.1039/C3CP50799H.

[111] Zolot AM, Giorgetta FR, Baumann E, Swann WC, Coddington I, Newbury NR. Broad-band frequency references in the near-infrared: Accurate dual comb spectroscopy of methane and acetylene. J Quant Spectrosc Radiat Transfer 2013;118:26–39. http://dx.doi.org/10.1016/j.jqsrt.2012.11.024.

[112] Delahaye T, Maxwell SE, Reed ZD, Lin H, Hodges JT, Sung K, et al. Precise methane absorption measurements in the 1.64 spectral region for the MERLIN mission. J Geophys Res: Atmos 2016;121:7360–70. http://dx.doi.org/10.1002/2016JD025024.

[113] Hashemi R, Predoi-Cross A, Nikitin AV, Tyuterev VG, Sung K, Smith MAH, et al. Spectroscopic line parameters of $^{12}CH_4$ for atmospheric composition retrievals in the 4300-4500 cm^{-1} region. J Quant Spectrosc Radiat Transfer 2017;186:106–17. http://dx.doi.org/10.1016/j.jqsrt.2016.03.024.

[114] Ghysels M, Mondelain D, Kassi S, Nikitin A, V, Rey M, et al. The methane absorption spectrum near 1.73μm (5695-5850 cm^{-1}): Empirical line lists at 80 K and 296 K and rovibrational assignments. J Quant Spectrosc Radiat Transfer 2018;213:169–77. http://dx.doi.org/10.1016/j.jqsrt.2018.04.007.

[115] Gotti R, Prevedelli M, Kassi S, Marangoni M, Romanini D. Feed-forward coherent link from a comb to a diode laser: Application to widely tunable cavity ring-down spectroscopy. J Chem Phys 2018;148:054202. http://dx.doi.org/10.1063/1.5018611.

[116] Kocheril PA, Markus CR, Esposito AM, Schrader AW, Dieter TS, McCall BJ. Extended sub-Doppler resolution spectroscopy of the ν_3 band of methane. J Quant Spectrosc Radiat Transfer 2018;215:9–12. http://dx.doi.org/10.1016/j.jqsrt.2018.04.033.

[117] Tyuterev V, Tashkun S, Rey M, Kochanov R, Nikitin A, Delahaye T. Accurate spectroscopic models for methane polyads derived from a potential energy surface using high-order contact transformations. J Phys Chem A 2013;117:13779–805. http://dx.doi.org/10.1021/jp408116j.

[118] Yang L, Lin H, Feng XJ, Zhang JT. Temperature-scanning saturation cavity ring-down spectrometry for doppler-free spectroscopy. Opt Express 2018;26:10203–10. http://dx.doi.org/10.1364/OE.26.010203.

[119] Lin H, Yang L, Feng XJ, Zhang JT. Discovery of new lines in the R9 multiplet of the $2\nu_3$ band of $^{12}CH_4$. Phys Rev Lett 2019;122:013002.

[120] Yang L, Lin H, Feng XJ, Plimmer MD, Zhang JT. Saturation cavity ring-down spectrometry using a dynamical relaxation model. Opt Express 2019;27:1769–76. http://dx.doi.org/10.1364/OE.27.001769.

[121] Campargue A, Leshchishina O, Mondelain D, Kassi S, Coustenis A. An improved empirical line list for methane in the region of the $2\nu_3$ band at 1.66μm. J Quant Spectrosc Radiat Transfer 2013;118:49–59. http://dx.doi.org/10.1016/j.jqsrt.2012.12.004.

[122] Yang L, Lin H, Plimmer M, Feng X-J, Ma Y-J, Luo J-T, et al. Measurement of the spectral line positions in the $2\nu_3$ R(6) manifold of methane. J Quant Spectrosc Radiat Transfer 2020;245:106888. http://dx.doi.org/10.1016/j.jqsrt.2020.106888.

[123] Okubo S, Inaba H, Okuda S, Sasada H. Frequency measurements of the $2\nu_3$ A_1 – ν_3 band transitions of methane in comb-referenced infrared-infrared double-resonance spectroscopy. Phys Rev A 2021;103:022809. http://dx.doi.org/10.1103/PhysRevA.103.022809.

[124] Foltynowicz A, Rutkowski L, Silander I, Johansson AC, Silva de Oliveira V, Axner O, et al. Measurement and assignment of double-resonance transitions to the 8900–9100 cm^{-1} levels of methane. Phys Rev A 2021;103:022810. http://dx.doi.org/10.1103/PhysRevA.103.022810.

[125] Champion J-P, Berger H. A. Spectre Raman à haute résolution de la bande ν_2 de $^{12}CH_4$. J Physique 1975;36:135–9.

[126] Gray DL, Robiette AG. Simultaneous analysis of the ν_2 and ν_4 bands of methane. Mol Phys 1976;32:1609–25. http://dx.doi.org/10.1080/00268977600102941.

[127] Champion J-P. Développement complet de l'hamiltonien de vibration–rotation adapté à l'étude des interactions dans les molécules toupies sphériques. Application aux bandes ν_2 et ν_4 de $^{12}CH_4$. Can J Phys 1977;55:1802–28.

[128] Bermejo D, Santos J, Cancio P. High-resolution Q-cw SRS spectrum of $^{12}CH_4$ in the region of the level-crossing between ν_1 and $\nu_2 + \nu_4$. J Mol Spectrosc 1992;156:303–6.

[129] Millot G, Lavorel B, Steinfeld JI. Collisional broadening, line shifting, and line mixing in the stimulated raman $2\nu_2$ Q-branch of CH_4. J Chem Phys 1991;95:7938–46. http://dx.doi.org/10.1063/1.461322.

[130] Hilico JC, Champion JP, Toumi S, Tyuterev VG, Tashkun SA. New analysis of the pentad system of methane and prediction of the (pentad-pentad) spectrum. J Mol Spectrosc 1994;168:455–76. http://dx.doi.org/10.1006/jmsp.1994.1293.

[131] Santos J, Cancio P, Domenech JL, Rodriguez J, Bermejo D. Accurate wave-number measurement in high-resolution stimulated Raman-spectroscopy (srs) by using an infrared standard nu fundamental of $^{12}CH_4$. Laser Chem 1992;12:53–63.

[132] Kozlov DN, Prokhorov AM, Smirnov VV. Methane-$\nu_1(A_1)$ vibrational-state rotational structure obtained from high-resolution CARS-spectra of the Q-branch. J Mol Spectrosc 1979;77:21–8. http://dx.doi.org/10.1016/0022-2852(79)90191-7.

[133] Graener H, Laubereau A. High-Resolution Fourier-Transform Raman-Spectroscopy with Ultrashort Laser-Pulses. Opt Comms 1985;54:141–6. http://dx.doi.org/10.1016/0030-4018(85)90279-2.

[134] Thiery MM, Fabre D, Kobashi K. Raman-Spectra of Solid CH_4 under High-Pressure. III. New High-Pressure Phases in Solid CH_4 and CD_4. J Chem Phys 1985;83:6165–72. http://dx.doi.org/10.1063/1.449612.

[135] Owyoung A, Patterson CW, McDowell RS. CW stimulated raman gain spectroscopy of the υ_4 fundamental of methane. Chem Phys Lett 1978;59:156–62.

[136] Clements WR, Stoicheff BP. High-resolution Raman spectroscopy of gases with laser excitation. J Mol Spectrosc 1970;33:183. http://dx.doi.org/10.1016/0022-2852(70)90066-4.

[137] Champion J-P. B. Analyse de la bande fondamentale ν_2 de $^{12}CH_4$. J Physique 1975;36:141–51.

[138] May AD, Henesian MA, Byer RL. The CW coherent anti-Stokes Raman spectrum of the ν_1 band of CH_4 and its pressure dependence. Can J Phys 1978;56:248–50.

[139] Magnotti G, Kc U, Varghese PL, Barlow RS. Raman spectra of methane, ethylene, ethane, dimethyl ether, formaldehyde and propane for combustion applications. J Quant Spectrosc Radiat Transfer 2015;163:80–101. http://dx.doi.org/10.1016/j.jqsrt.2015.04.018.

[140] Berger H. Raman spectrum of $^{12}CH_4$ between 2850 and 3100 cm^{-1}. J Mol Spectrosc 1977;66:55–61. http://dx.doi.org/10.1016/0022-2852(77)90320-4.

[141] Champion JP, Pierre G, Berger H, Cadot J. Vibration–rotation energies of harmonic and combination levels in tetrahedral XY_4 molecules - analysis of the $2\nu_2$ and $\nu_2 + \nu_4$ bands of $^{12}CH_4$. J Mol Spectrosc 1980;79:281–94. http://dx.doi.org/10.1016/0022-2852(80)90214-3.

[142] Frunder H, Illig D, Finsterholzl H, Schrotter HW, Lavorel B, Roussel G, et al. Revised analysis of the structure of the ν_1 band of methane. Chem Phys Lett 1983;100:110–4. http://dx.doi.org/10.1016/0009-2614(83)87273-X.

[143] Jourdanneau E, Chaussard F, Saint-Loup R, Gabard T, Berger H. The methane Raman spectrum from 1200 to 5500 cm^{-1}: A first step toward temperature diagnostic using methane as a probe molecule in combustion systems. J Mol Spectrosc 2005;233:219–30. http://dx.doi.org/10.1016/j.jms.2005.07.004.

[144] Lolck JE, Brodersen S, Robiette AG. The $2\nu_4$ isotropic and anisotropic Raman bands of CH_4. J Raman Spectrosc 1982;12(1):49–62. http://dx.doi.org/10.1002/jrs.1250120108.

[145] Jourdanneau E, Gabard T, Chaussard F, Saint-Loup R, Berger H, Bertseva E, et al. CARS methane spectra: Experiments and simulations for temperature diagnostic purposes. J Mol Spectrosc 2007;246:167–79. http://dx.doi.org/10.1016/j.jms.2007.09.006.

[146] Ba YA, Wenger C, Surleau R, Boudon V, Rotger M, Daumont L, et al. MeCaSDa and ECaSDa: Methane and ethene calculated spectroscopic databases for the virtual atomic and molecular data centre. J Quant Spectrosc Radiat Transfer 2013;130:62–8. http://dx.doi.org/10.1016/j.jqsrt.2013.05.001, HITRAN2012 special issue..

[147] Itano WM, Ozier I. Avoided-crossing molecular-beam spectroscopy of methane. J Chem Phys 1980;72:3700–11. http://dx.doi.org/10.1063/1.439581.

[148] Curl RF. Infrared-radio frequency double-resonance observations of pure rotational Q-branch transitions of methane. J Mol Spectrosc 1973;48:165–73. http://dx.doi.org/10.1016/0022-2852(73)90145-8.

[149] Oldani M, Andrist M, Bauder A, Robiette AG. Pure rotational spectra of methane and methane-D4 in the vibrational ground state observed by microwave Fourier transform spectroscopy. J Mol Spectrosc 1985;110:93–105.

[150] Holt CW, Gerry MCL, Ozier I. Microwave spectrum of $^{12}CH_4$ in the ground vibronic state. Phys Rev Lett 1973;31:1033–6.

[151] Oldani M, Bauder A, Hilico JC, Loete M, Champion JP. Microwave Fourier-transform spectroscopy of rovibrational transitions in the $\nu_2 - \nu_4$ dyads of methane-^{12}C and methane-^{13}C. Europhys Lett 1987;4:29–33. http://dx.doi.org/10.1209/0295-5075/4/1/005.

[152] Takami M, Uehara K, Shimoda K. Rotational transitions of CH_4 in $\nu_3 = 1$ excited-state observed by an infrared-microwave double-resonance method. Japanese J Appl Phys 1973;12:924–5. http://dx.doi.org/10.1143/JJAP.12.924.

[153] Holt CW, Gerry MCL, Ozier I. The distortion moment microwave spectrum of $^{12}CH_4$ in the ground vibronic state. Can J Phys 1975;53:1791–805.

[154] Hilico JC, Loete L, Champion JP, Destomes JL, Bogey M. The millimeter-wave spectrum of methane. J Mol Spectrosc 1987;122:381–9.

[155] Bray C, Cuisset A, Hindle F, Mouret G, Bocquet R, Boudon V. Spectral lines of methane measured up to 2.6 THz at sub-MHz accuracy with a CW-THz photomixing spectrometer: Line positions of rotational transitions induced by centrifugal distortion. J Quant Spectrosc Radiat Transfer 2017;203:349–54. http://dx.doi.org/10.1016/j.jqsrt.2017.04.010.

[156] Boudon V, Pirali O, Roy P, Brubach J-B, Manceron L, Vander Auwera J. The high-resolution far-infrared spectrum of methane at the SOLEIL synchrotron. J Quant Spectrosc Radiat Transfer 2010;111:1117–29.

[157] Smith MAH, Benner DC, Predoi-Cross A, Devi VM. Multispectrum analysis of $^{12}CH_4$ in the nu(4) spectral region: II. Self-broadened half widths, pressure-induced shifts, temperature dependences and line mixing. J Quant Spectrosc Radiat Transf 2010;111:1152–66. http://dx.doi.org/10.1016/j.jqsrt.2010.01.017.

[158] Germann M, Hjalten A, Boudon V, Richard C, Krzempek K, Hudzikowski A, et al. A methane line list with sub-MHz accuracy in the 1250 to 1380 cm^{-1} range from optical frequency comb Fourier transform spectroscopy. J Quant Spectrosc Radiat Transfer 2022;288:108252. http://dx.doi.org/10.1016/j.jqsrt.2022.108252.

[159] Hilico JC, Baronov GS, Bronnikov DK, Gavrikov SA, Nikolaev II, Rusanov VD, et al. High-resolution spectroscopy of (pentad–dyad) and (octad–pentad) hot bands of methane in a supersonic jet. J Mol Spectrosc 1993;161:435–44.

[160] Restelli G, Cappellani F. High resolution spectroscopy of the ν_4 band of methane. J Mol Spectrosc 1979;78:161–9.

[161] Hilico JC, Loete M, Brown LR. Line strengths of the $\upsilon_3+\upsilon_3$ and $\upsilon_3-\upsilon_3$ bands of methane ($^{12}CH_4$). J Mol Spectrosc 1992;152:229–51.

[162] Li J, Ding Y, Li Z, Peng Z. Quantum cascade laser measurements of CH_4 linestrength and temperature-dependent self-broadening and narrowing parameters at 7.16μm. J Quant Spectrosc Radiat Transfer 2021;276:107901. http://dx.doi.org/10.1016/j.jqsrt.2021.107901.

[163] Smith MAH, Benner DC, Predoi-Cross A, Devi VM. Air- and self-broadened half widths, pressure-induced shifts, and line mixing in the ν_2 band of $^{12}CH_4$. J Quant Spectrosc Radiat Transfer 2014;133:217–34. http://dx.doi.org/10.1016/j.jqsrt.2013.08.004.

[164] Baumann E, Giorgetta FR, Swann WC, Zolot AM, Coddington I, Newbury NR. Spectroscopy of the methane ν_3 band with an accurate midinfrared coherent dual-comb spectrometer. Phys Rev A 2011;84:062513. http://dx.doi.org/10.1103/PhysRevA.84.062513.

[165] Okubo S, Nakayama H, Iwakuni K, Inaba H, Sasada H. Absolute frequency list of the ν_3-band transitions of methane at a relative uncertainty level of 10^{-11}. Opt Express 2011;19:23878–88. http://dx.doi.org/10.1364/OE.19.023878.

[166] Takahata K, Kobayashi T, Sasada H, Nakajima Y, Inaba H, Hong F-L. Absolute frequency measurement of sub-doppler molecular lines using a 3.4−μm difference-frequency-generation spectrometer and a fiber-based frequency comb. Phys Rev A 2009;80:032518. http://dx.doi.org/10.1103/PhysRevA.80.032518.

[167] Liu J, Riyadh SM, Telfah H, Jones I, Bersson J, Cheng C, et al. Mid-infrared doppler-free saturation absorption spectroscopy of the Q branch of CH_4 $\nu_3=1$ band using a rapid-scanning continuous-wave optical parametric oscillator. Optica Open 2000. http://dx.doi.org/10.1364/opticaopen.22138301.v1.

[168] Pine AS. Speed-dependent line mixing in the ν_3 band Q branch of methane. J Quant Spectrosc Radiat Transfer 2019;224:62–77. http://dx.doi.org/10.1016/j.jqsrt.2018.10.038.

[169] Grigoriev IM, Filippov NN, Tonkov MV, Champion JP, Gabard T, Le Doucen R. Line parameters and shapes of high clusters: R branch of the ν_3 band of CH_4 in He mixtures. J Quant Spectrosc Radiat Transfer 2002;74:431–43.

[170] Rodina AA, Nikitin AV, Thomas X, Manceron L, Daumont L, Rey M, et al. Improved line list of $^{12}CH_4$ in the 3760–4100 cm^{-1} region. J Quant Spectrosc Radiat Transfer 2019;225:351–62. http://dx.doi.org/10.1016/j.jqsrt.2018.12.034.

[171] Hilico J-C, Robert O, Loëte M, Toumi S, Pine AS, Brown LR. Analysis of the interacting octad system of $^{12}CH_4$. J Mol Spectrosc 2001;208:1–13. http://dx.doi.org/10.1006/jmsp.2001.8364.

[172] Rodina AA, Nikitin A, V, Manceron L, Thomas X, Daumont L, et al. Improved line list of $^{12}CH_4$ in the 4100-4300 cm^{-1} region. J Quant Spectrosc Radiat Transfer 2022;279:108021. http://dx.doi.org/10.1016/j.jqsrt.2021.108021.

[173] Nikitin AV, Rodina AA, Thomas X, Manceron L, Daumont L, Rey M, et al. Line list of $^{12}CH_4$ in the 4300–4600 cm^{-1} region. J Quant Spectrosc Radiat Transfer 2020;253:107061. http://dx.doi.org/10.1016/j.jqsrt.2020.107061.

[174] Devi VM, Benner DC, Smith MAH, Mantz AW, Sung K, Crawford TJ, et al. Self- and air-broadened line shape parameters in the $\nu_2+\nu_3$ band of $^{12}CH_4$: 4500-4630 cm^{-1}. J Quant Spectrosc Radiat Transfer 2015;152:149–65. http://dx.doi.org/10.1016/j.jqsrt.2014.11.011.

[175] Daumont L, Nikitin AV, Thomas X, Regalia L, Von der Heyden P, Tyuterev VG, et al. New assignments in the 2μm transparency window of the $^{12}CH_4$ Octad band system. J Quant Spectrosc Radiat Transfer 2013;116:101–9. http://dx.doi.org/10.1016/j.jqsrt.2012.08.025.

[176] Nikitin A, Thomas X, Régalia L, Daumont L, Rey M, Tashkun S, et al. Measurements and modeling of long-path $^{12}CH_4$ spectra in the 4800–5300 cm^{-1} region. J Quant Spectrosc Radiat Transfer 2014;138:116–23. http://dx.doi.org/10.1016/j.jqsrt.2014.02.005.

[177] Robert O, Hilico JC, Loete M, Champion JP, Brown LR. First assignment and line strengths of the $4\nu_4$ band of $^{12}CH_4$ near 1.9μm. J Mol Spectrosc 2001;209:14–23.

[178] Ma H, Zha S, Cai X, Lin G, Cao Z. Line parameters of $^{12}CH_4$ around 2.008μm studied by tunable diode laser spectroscopy with a long-path White cell. J Opt Soc Amer B 2018;35:2453–8. http://dx.doi.org/10.1364/JOSAB.35.002453.

[179] Nikitin AV, Thomas X, Daumont L, Rey M, Sung K, Toon GC, et al. Measurements and modeling of long-path $^{12}CH_4$ spectra in the 5300-5550 cm^{-1} region. J Quant Spectrosc Radiat Transfer 2017;202:255–64. http://dx.doi.org/10.1016/j.jqsrt.2017.07.030.

[180] Nikitin VA, Thomas X, Daumont L, Rey M, Sung K, Toon GC, et al. Assignment and modelling of $^{12}CH_4$ spectra in the (5718) 5550-5695-5725 and 5792-5814 cm^{-1} regions. J Quant Spectrosc Radiat Transfer 2018;219:323–32. http://dx.doi.org/10.1016/j.jqsrt.2018.08.006.

[181] Lyulin OM, Nikitin AV, Perevalov VI, Morino I, Yokota T, Kumazawa R, et al. Measurements of N_2- and O_2-broadening and shifting parameters of methane spectral lines in the 5550–6236 cm^{-1} region. J Quant Spectrosc Radiat Transfer 2009;110:654–68. http://dx.doi.org/10.1016/j.jqsrt.2009.02.012.

[182] Georges R, Herman M, Hilico JC, Robert O. High-resolution FTIR spectroscopy using a jet: Sampling the rovibrational spectrum of $^{12}CH_4$. J Mol Spectrosc 1998;187:13–20.

[183] Dudás E, Vispoel B, Gamache RR, Rey M, Tyuterev VG, Nikitin AV, et al. Non-LTE spectroscopy of the tetradecad region of methane recorded in a hypersonic flow. Icarus 2023;394:115421. http://dx.doi.org/10.1016/j.icarus.2022.115421.

[184] Nikitin AV, Thomas X, Regalia L, Daumont L, Von der Heyden P, Tyuterev VG, et al. First assignment of the $5\nu_4$ and $\nu_2+4\nu_4$ band systems of $^{12}CH_4$ in the 6287-6550 cm^{-1} region. J Quant Spectrosc Radiat Transfer 2011;112:28–40. http://dx.doi.org/10.1016/j.jqsrt.2010.08.006.

[185] Nikitin AV, Protasevich AE, Rey M, Serdyukov VI, Sinitsa LN, Lugovskoy A, et al. Improved line list of $^{12}CH_4$ in the 8850-9180 cm^{-1} region. J Quant Spectrosc Radiat Transfer 2019;239:106646. http://dx.doi.org/10.1016/j.jqsrt.2019.106646.

[186] Nelson RC, Plyler EK, Benedict WS. Absorption spectra of methane in the near infrared. J Res Natl Bur Stand 1948;41:615–21. http://dx.doi.org/10.6028/jres.041.049.

[187] Boyd DRJ, Thompson HW, Williams RL. Vibration–rotation bands of methane. Proc R Soc Lond Ser A Math Phys Eng Sci 1952;213:42–54. http://dx.doi.org/10.1098/rspa.1952.0109.

[188] Feldman T, Romanko J, Welsh HL. The ν_2 Raman band of methane. Can J Phys 1955;33:138–45. http://dx.doi.org/10.1139/p55-018.

[189] Rank DH, Eastman DP, Skorinko G, Wiggins TA. Fine structure in the lines of the $2\nu_3$ band of methane. J Mol Spectrosc 1960;5:78–82. http://dx.doi.org/10.1016/0022-2852(61)90069-8.

[190] Moretbailly J, Gautier L, Montagutelli J. Cebsch-gordan coefficients adapted to cubic symmetry. J Mol Spectrosc 1965;15. http://dx.doi.org/10.1016/0022-2852(65)90151-7, 355+.

[191] Moret-Bailly J. Calculation of the frequencies of the lines in a threefold degenerate fundamental band of a spherical top molecule. J Mol Spectrosc 1965;15:344–54.

[192] Herranz J, Morcillo J, Gómez A. The ν_2 infrared band of CH_4 and CD_4. J Mol Spectrosc 1966;19:266–82.

[193] McDowell RS. The ν_3 infrared bands of $^{12}CH_4$ and$^{13}CH_4$. J Mol Spectrosc 1966;21:280–90.

[194] Henry L, Husson N, Andia R, Valentin A. Infrared absorption spectrum of methane from 2884 cm^{-1} to 3141 cm^{-1}. J Mol Spectrosc 1970;36:511. http://dx.doi.org/10.1016/0022-2852(70)90224-9.

[195] Ozier I, Yi PN, Khosla A, Ramsey NF. Direct observation of ortho-para transitions in methane. Phys Rev Lett 1970;24:642. http://dx.doi.org/10.1103/PhysRevLett.24.642.

[196] Husson N, Nhu MD. Analyse rotationnelle de la bande ν_3 de $^{12}CH_4$ de 2884 a 3141 cm^{-1}. J Physique 1971;32:627–38.

[197] Husson N, Poussigue G. Analyse rotationnelle de la bande ν_4 de $^{12}CH_4$ de 1225 à 1376 cm^{-1}. J Physique 1971;32:859–65.

[198] Barnes WL, Susskind J, Hunt RH, Plyler EK. Measurement and analysis of the ν_3 band of methane. J Chem Phys 1972;56:5160–72.

[199] Bobin B. Interpretation of $2\upsilon_3$ harmonic band of methane $^{12}CH_4$ (from 5890 to 6107 cm^{-1}). J Phys 1972;33:345–52.

[200] Rosenberg A, Ozier I, Kudian AK. Pure rotational spectrum of CH_4. J Chem Phys 1972;57. http://dx.doi.org/10.1063/1.1678001, 568+.

[201] Berger H, Faivre M, Champion JP, J M-B. High-resolution raman spectroscopy of CH_4. J Mol Spectrosc 1973;45:298–301. http://dx.doi.org/10.1016/0022-2852(73)90161-6.

[202] Bobin B, Fox K. Nouvelle interprétation de la bande νs de $^{12}CH_4$, de 2840 à 3167 cm^{-1}. J Phys 1973;34:571–82.

[203] Cadot J, Delorme R. Experimental determination of J values for some lines of bands $\nu_2+\nu_3$ and $\nu_3+\nu_4$ of methane. J Mol Spectrosc 1973;45:443–9. http://dx.doi.org/10.1016/0022-2852(73)90215-4.

[204] Curl RF, Oka T, Smith DS. Observation of a pure rotational Q-branch transition of methane by infrared-radio frequency double-resonance. J Mol Spectrosc 1973;46:518–20. http://dx.doi.org/10.1016/0022-2852(73)90066-0.

[205] Darnton L, Margolis JS. The temperature dependence of the half widths of some self-and foreign-gas-broadened lines of methane. J Quant Spectrosc Radiat Transfer 1973;13:969–76.

[206] Susskind J. Analysis of the ν_4 band of CH_4. J Mol Spectrosc 1973;45:457–66.

[207] Berger H. Simultaneous Study of Vibrational Band-ν_2 and Band-ν_4 of Spherical Tops, Using Irreducible Tensors of O_3. J Mol Spectrosc 1975;55:48–55. http://dx.doi.org/10.1016/0022-2852(75)90250-7.

[208] Bobin B, Hilico JC. Attribution des transitions du type ($R'=J'\pm2\leftarrow J_0$) de la bande ($\nu_3+\nu_4$) du méthane $^{12}CH_4$. J Physique 1975;36:225–33.

[209] Rosenberg A, Ozier I. The forbidden ($J\rightarrow J+1$) spectrum of CH_4 in the ground vibronic state. J Mol Spectrosc 1975;56:124–32.

[210] Tarrago G, Dang-Nhu M, Poussigue G, Guelachvili G, Amiot C. The ground state of methane $^{12}CH_4$ through the forbidden lines of the ν_3 band. J Mol Spectrosc 1975;57:246–63.

[211] Hall JL, Bordé CJ, Uehara K. Direct optical resolution of the recoil effect using saturated absorption spectroscopy. Phys Rev Lett 1976;37:1339–42. http://dx.doi.org/10.1103/PhysRevLett.37.1339.

[212] Aliev MR, Kozlov DN, Smirnov VV. Coherent spectroscopy of high-resolution Raman-scattering of methane. JETP Lett 1977;26:27–9.

[213] Toth RA, Brown LR, Hunt RH. Line positions and strengths of methane in the 2862 to 3000 cm^{-1} region. J Mol Spectrosc 1977;67:1–33. http://dx.doi.org/10.1016/0022-2852(77)90031-5.

[214] Bobin B, Guelachvili G. Analyse de la bande de combinaison (ν_3+ ν_4) du méthane $^{12}CH_4$. J Physique 1978;39:33–42.

[215] Chedin A, Husson N, Scott NA, Gautier D. ν4 band of methane ($^{12}CH_4$ and $^{13}CH_4$). Line parameters and evaluation of Jovian atmospheric transmission at 7.7μm. J Mol Spectrosc 1978;71:343–68.

[216] Hunt RH, Brown LR, Toth RA. Line intensities of methane in the 2700–2862-cm^{-1} region. J Mol Spectrosc 1978;69:482–5.

[217] Ozier I, Rosenberg A. The vibrationally induced rotational spectrum of CH_4 in the $\upsilon_4 = 1$ state. J Chem Phys 1978;69:5203–4.

[218] Blatherwick RD, Goldman A, Lutz B, Silvaggio PM, Boese RW. Infrared methane spectra between 1120 cm^{-1} and 1800 cm^{-1}: a new atlas. Appl Opt 1979;18:3798–804.

[219] Boquillon JP, Bregier R. igh-resolution coherent stokes raman-spectroscopy of the ν_1 and ν_3 bands of methane. Appl Phys 1979;18:195–8. http://dx.doi.org/10.1007/BF00934415.

[220] Gray DL, Robiette AG. The anharmonic force field and equilibrium structure of methane. Mol Phys 1979;37:1901–20. http://dx.doi.org/10.1080/00268977900101401.

[221] Gray DL, Robiette AG, Pine AS. Extended measurement and analysis of the ν_3-infrared band of methane. J Mol Spectrosc 1979;77:440–56. http://dx.doi.org/10.1016/0022-2852(79)90183-8.

[222] Hilico JC, Degni J, Champion JP, Guelachvili G. Analysis of the $\nu_2 + \nu_3$ band of $^{12}CH_4$ and $^{13}CH_4$. J Mol Spectrosc 1980;81:277–302.

[223] Jennings DE. Intermode calibration of diode-laser spectra using tandem étalons. Appl Opt 1980;19:2–4. http://dx.doi.org/10.1364/AO.19.000002.

[224] Orton GS, Robiette AG. A line parameter list for the υ_2 and υ_4 bands of $^{12}CH_4$ and $^{13}CH_4$, extended to $j' = 25$ and its application to planetary-atmospheres. J Quant Spectrosc Radiat Transfer 1980;24:81–95. http://dx.doi.org/10.1016/0022-4073(80)90023-0.

[225] Valentini JJ, Esherick P, Owyoung A. Use of a free-expansion jet in ultra-high-resolution inverse Raman-spectroscopy. Chem Phys Lett 1980;75:590–2. http://dx.doi.org/10.1016/0009-2614(80)80586-0.

[226] Gherissi S, Henry A, Loete M, Valentin A. Transition-moment and line strengths of the ν_3 Band of $^{12}CH_4$. J Mol Spectrosc 1981;86:344–56. http://dx.doi.org/10.1016/0022-2852(81)90286-1.

[227] Hunt RH, Brown LR, Toth RA, Brault JW. Line assignments and intensities for the $\nu_3 + \nu_4 - \nu_4$ Band of $^{12}CH_4$. J Mol Spectrosc 1981;86:170–83.

[228] Ozler I, Gerry MCL, Robiette AG. Microwave-spectra of molecules of astrophysical interest.20. Methane. J Phys Chem Ref Data 1981;10(4):1085–95.

[229] Robiette AG. Extended assignment and analysis of the ν_2 and ν_4 infrared bands of $^{12}CH_4$. J Mol Spectrosc 1981;86:143–58. http://dx.doi.org/10.1016/0022-2852(81)90113-2.

[230] Toth RA, Brown LR, Hunt RH, Rothman LS. Line parameters of methane from 2385 to 3200 cm^{-1}. Appl Opt 1981;20:932–5. http://dx.doi.org/10.1364/AO.20.000932.

[231] Brown LR, Rothman LS. Methane line parameters for the 2.3μm region. Appl Opt 1982;21:2425–7.

[232] Brown LR, Toth RA, Robiette AG, Lolck J, Hunt RH, Brault JW. Analysis of the ν_1 and $\nu_2 + \nu_4$ bands of $^{12}CH_4$. J Mol Spectrosc 1982;93:317–50. http://dx.doi.org/10.1016/0022-2852(82)90171-0.

[233] Lutz BL, Pierre C, Pierre G, Champion JP. Quantum assignments and intensity measures for methane between 1100 and 1800 cm^{-1} - a comparison between theory and experiment. Astrophys J Suppl 1982;48:507–30. http://dx.doi.org/10.1086/190787.

[234] Restelli G, Cappellani F. Tunable diode-laser measurements of spectral intensities in the ν_4 band of $^{12}CH_4$. Chem Phys Lett 1982;92:439–42. http://dx.doi.org/10.1016/0009-2614(82)83445-3.

[235] Poussigue G, Pascaud E, Champion JP, Pierre G. Rotational analysis of vibrational polyads in tetrahedral molecules - simultaneous analysis of the pentad energy-levels of $^{12}CH_4$. J Mol Spectrosc 1982;93:351–80. http://dx.doi.org/10.1016/0022-2852(82)90172-2.

[236] Brown LR, Margolis JS, Norton RH, Stedry BD. Computer measurement of line strengths with application to the methane spectrum. Appl Spectrosc 1983;37:287–92. http://dx.doi.org/10.1366/0003702834634514.

[237] Varanasi P, Giver LP, Valero FPJ. Intensity measurements in the ν_4-fundamental of $^{13}CH_4$ at planetary atmospheric temperatures. J Quant Spectrosc Radiat Transfer 1983;30:491–5. http://dx.doi.org/10.1016/0022-4073(83)90002-X.

[238] Brown LR, Toth RA. Comparison of the frequencies of NH_3, CO_2, H_2O, N_2O, CO, and CH_4 as infrared calibration standards. J Opt Soc Am B 1985;2:842–56. http://dx.doi.org/10.1364/JOSAB.2.000842.

[239] Keffer CE, Conner CP, Smith WH. Pressure broadening of methane lines in the 6190 Å and 6825 Å bands at room and lowtemperatures. J Quant Spectrosc Radiat Transfer 1986;35:495–9. http://dx.doi.org/10.1016/0022-4073(86)90038-5.

[240] Kim K. Integrated infrared intensities of methane. J Quant Spectrosc Radiat Transfer 1987;37:107–10. http://dx.doi.org/10.1016/0022-4073(87)90013-6.

[241] Tyuterev VG, Champion JP, Pierre G, Perevalov VI. Parameters of reduced hamiltonian and invariant parameters of interacting E and F_2 fundamentals of tetrahedral molecules - ν_2 and ν_4 bands of $^{12}CH_4$ and $^{28}Si_4$. J Mol Spectrosc 1986;120:49–78. http://dx.doi.org/10.1016/0022-2852(86)90070-6.

[242] Brown LR, Loete M, Hilico JC. Linestrengths of the ν_2 and ν_4 Bands of $^{12}CH_4$ and $^{13}CH_4$. J Mol Spectrosc 1989;133:273–311. http://dx.doi.org/10.1016/0022-2852(89)90194-X.

[243] Varanasi P, Chudamani S. Measurements of collision-broadened line widths in the ν_4-fundamental band of $^{12}CH_4$ at low temperatures. J Quant Spectrosc Radiat Transfer 1989;41:335–43. http://dx.doi.org/10.1016/0022-4073(89)90062-9.

[244] Varanasi P, Chudamani S. The temperature-dependence of lineshifts, linewidths and line-intensities of methane at low-temperatures. J Quant Spectrosc Radiat Transfer 1990;43:1–11. http://dx.doi.org/10.1016/0022-4073(90)90060.

[245] Roche C, Champion JP. Analysis of dyad - dyad transitions of $^{12}CH_4$ and $^{13}CH_4$. Can J Phys 1991;69:40–51. http://dx.doi.org/10.1139/p91-007.

[246] Brown LR, Margolis JS, Champion JP, Hilico JC, Jouvard JM, Loete M, et al. Methane and its isotopes - current status and prospects for improvement. J Quant Spectrosc Radiat Transfer 1992;48:617–28. http://dx.doi.org/10.1016/0022-4073(92)90126-O.

[247] Pine AS. Self-broadening, N_2-broadening, O_2-broadening, H_2-broadening, Ar-broadening, and He-broadening in the ν_3 band Q-branch of CH_4. J Chem Phys 1992;97:773–85.

[248] Smith MAH, Rinsland CP, Devi VM, Benner DC. Temperature-dependence of broadening and shifts of methane lines in the ν_4 band. Spectra Chimica Acta A 1992;48:1257–72. http://dx.doi.org/10.1016/0584-8539(92)80263-V.

[249] Ouardi O, Hilico JC, Loete M, Brown LR. The hot bands of methane between 5 and 10μm. J Mol Spectrosc 1996;180:311–22. http://dx.doi.org/10.1006/jmsp.1996.0254.

[250] Wenger C, Champion JP. Spherical top data system (STDS) software for the simulation of spherical top spectra. J Quant Spectrosc Radiat Transfer 1998;59:471–80. http://dx.doi.org/10.1016/S0022-4073(97)00106-4.

[251] Menard-Bourcin F, Doyennette L, Menard J, Boursier C. Time-resolved IR-IR double resonance measurements in methane excited to $2\nu_3$(F-2). J Phys Chem 2000;104:5444–59.

[252] Nauta K, Miller RE. Rotational and vibrational dynamics of methane in helium nanodroplets. Chem Phys Lett 2001;350:225–32. http://dx.doi.org/10.1016/S0009-2614(01)01294-5.

[253] O'Brien JJ, Cao H. Absorption spectra and absorption coefficients for methane in the 750-940 nm region obtained by intracavity laser spectroscopy. J Quant Spectrosc Radiat Transfer 2002;75:323–50. http://dx.doi.org/10.1016/S0022-4073(02)00015-8.

[254] Gharavi M, Buckley SG. Diode laser absorption spectroscopy measurement of linestrengths and pressure broadening coefficients of the methane $2\nu_3$ band at elevated temperatures. J Mol Spectrosc 2005;229:78–88. http://dx.doi.org/10.1016/j.jms.2004.07.016.

[255] Mondelain D, Chelin P, Valentin A, Hurtmans D, Camy-Peyret C. Line profile study by diode laser spectroscopy in the $^{12}CH_4$ $\nu_2 + \nu_4$ band. J Mol Spectrosc 2005;233:23–31. http://dx.doi.org/10.1016/j.jms.2005.05.012.

[256] Boursier C, Menard J, Marquette A, Menard-Bourcin F. Identification of hot band transitions of CH_4 near 3000 cm^{-1}. J Mol Spectrosc 2006;237:104–14.

[257] Rudolph S, Wollny G, von Haeften K, Havenith M. Probing collective excitations in helium nanodroplets: Observation of phonon wings in the infrared spectrum of methane. J Chem Phys 2007;126:124318. http://dx.doi.org/10.1063/1.2709887.

[258] Wishnow EH, Orton GS, Ozier I, Gush HP. The distortion dipole rotational spectrum of CH_4: A low temperature far-infrared study. J Quant Spectrosc Radiat Transfer 2007;103:102–17. http://dx.doi.org/10.1016/j.jqsrt.2006.06.005.

[259] Hoshina H, Skvortsov D, Sartakov BG, Vilesov AF. Rotation of methane and silane molecules in He droplets. J Chem Phys 2010;132:074302. http://dx.doi.org/10.1063/1.3313925.

[260] Tran H, Hartmann J-M, Toon G, Brown LR, Frankenberg C, Warneke T, et al. The $2\nu_3$ band of CH_4 revisited with line mixing: Consequences for spectroscopy and atmospheric retrievals at 1.67μm. J Quant Spectrosc Radiat Transfer 2010;111(10):1344–56. http://dx.doi.org/10.1016/j.jqsrt.2010.02.015.

[261] Zillich RE, Whaley KB. Rotational spectra of methane and deuterated methane in helium. J Chem Phys 2010;132:174501. http://dx.doi.org/10.1063/1.3396002.

[262] Sanzharov M, Vander Auwera J, Pirali O, Roy P, Brubach J-B, Manceron L, et al. Self and N_2 collisional broadening of far-infrared methane lines measured at the SOLEIL synchrotron. J Quant Spectrosc Radiat Transfer 2012;113:1874–86.

[263] Zhang Y, Wang F-R, Zhao Y-H, Wang Y-D, Cui T, Kan R-W, et al. Experiment research on ellipsoidal structure methane using the absorption characteristics of 3.31μm mid-infrared spectroscopy. Infrared Phys Technol 2012;55:353–6. http://dx.doi.org/10.1016/j.infrared.2012.02.006.

[264] Rey M, Nikitin AV, Tyuterev VG. Theoretical hot methane line lists up to T=2000 K for astrophysical applications. Astrophys J 2014;789:2. http://dx.doi.org/10.1088/0004-637X/789/1/2.

[265] Liu K, Wang L, Tan T, Wang G, Zhang W, Chen W, et al. Highly sensitive detection of methane by near-infrared laser absorption spectroscopy using a compact dense-pattern multipass cell. Sensors Actuators B 2015;220:1000–5. http://dx.doi.org/10.1016/j.snb.2015.05.136.

[266] Nikitin AV, Protasevich AE, Rey M, Tyuterev VG. Highly excited vibrational levels of methane up to 10 300 cm^{-1}: Comparative study of variational methods (vol 149 124305, 2018). J Chem Phys 2018;149:159901. http://dx.doi.org/10.1063/1.5065469.

[267] Petrov DV. Raman spectrum of methane in nitrogen, carbon dioxide, hydrogen, ethane, and propane environments. Spectra Chimica Acta A 2018;191:573–8. http://dx.doi.org/10.1016/j.saa.2017.10.058.

[268] Rey M, Nikitin AV, Bezard B, Rannou P, Coustenis A, Tyuterev VG. New accurate theoretical line lists of $^{12}CH_4$ and $^{13}CH_4$ in the 0-13400 cm^{-1} range: Application to the modeling of methane absorption in Titan's atmosphere. Icarus 2018;303:114–30. http://dx.doi.org/10.1016/j.Icarus.2017.12.045.

[269] Butterworth TD, Amyay B, Bekerom DVD, Steeg AVD, Minea T, Gatti N, et al. Quantifying methane vibrational and rotational temperature with Raman scattering. J Quant Spectrosc Radiat Transfer 2019;236:106562. http://dx.doi.org/10.1016/j.jqsrt.2019.07.005.

[270] Delahaye T, Ghysels M, Hodges JT, Sung K, Armante R, Tran H. Measurement and modeling of air-broadened methane absorption in the MERLIN spectral region at low temperatures. J Geophys Res: Atmos 2019;124(6):3556–64. http://dx.doi.org/10.1029/2018JD028917.

[271] Gharib-Nezhad E, Heays AN, Bechtel HA, Lyons JR. H_2-induced pressure broadening and pressure shift in the P-branch of the ν_3 band of CH_4 from 300 to 655 K. J Quant Spectrosc Radiat Transfer 2019;239:106649. http://dx.doi.org/10.1016/j.jqsrt.2019.106649.

[272] Kiseleva M, Mandon J, Persijn S, Harren FJM. Accurate measurements of line strengths and air-broadening coefficients in methane around 1.66μm using cavity ring down spectroscopy. J Quant Spectrosc Radiat Transfer 2019;224:9–17. http://dx.doi.org/10.1016/j.jqsrt.2018.10.040.

[273] Gianella M, Nataraj A, Tuzson B, Jouy P, Kapsalidis F, Beck M, et al. High-resolution and gapless dual comb spectroscopy with current-tuned quantum cascade lasers. Opt Express 2020;28:6197–208. http://dx.doi.org/10.1364/OE.379790.

[274] Petrov VD, Matrosov II, Zaripov AR, Tanichev AS, Kobzev AA. Pressure dependence of peak position and shape of ν_1 methane Raman band. In: Matvienko GG, Romanovskii OA, editors. 26th International symposium on atmospheric and ocean optics, atmospheric physics. Proc. SPIE, vol. 11560, 2020, http://dx.doi.org/10.1117/12.2575639, 115600E.

[275] Cuisset A, Hindle F, Mouret G, Bocquet R, Bruckhuisen J, Decker J, et al. Terahertz rotational spectroscopy of greenhouse gases using long interaction path-lengths. Appl Sci 2021;11:1229. http://dx.doi.org/10.3390/app11031229.

[276] Farji A, Aroui H, Vander Auwera J. Air-induced collisional parameters in the ν_3 band of methane. J Quant Spectrosc Radiat Transfer 2021;275:107878. http://dx.doi.org/10.1016/j.jqsrt.2021.107878.

[277] Foltynowicz A, Rutkowski L, Silander I, Johansson AC, Silva de Oliveira V, Axner O, et al. Sub-Doppler double-resonance spectroscopy of methane using a frequency comb probe. Phys Rev Lett 2021;126:063001. http://dx.doi.org/10.1103/PhysRevLett.126.063001.

[278] t. Es-sebbar E, Farooq A. Line-strengths, collisional coefficients and narrowing parameters in the ν_3 band of methane: H_2, He, N_2, O_2, Ar and CO_2 collider effects. J Quant Spectrosc Radiat Transfer 2021;272:107758. http://dx.doi.org/10.1016/j.jqsrt.2021.107758.

[279] Zhu N, Xu Z, Wang Z, Song Z, Wang W, Chen X, et al. Midinfrared compressed fourier-transform spectroscopy with an optical frequency comb. Phys Rev A 2022;18:024025. http://dx.doi.org/10.1103/PhysRevApplied.18.024025.

[280] Mazza F, Thornquist O, Castellanos L, Butterworth T, Richard C, Boudon V, et al. The ro-vibrational ν_2 mode spectrum of methane investigated by ultrabroadband coherent Raman spectroscopy. J Chem Phys 2023;158:094201. http://dx.doi.org/10.1063/5.0138803.

[281] Vasilchenko S, Delahaye T, Kassi S, Campargue A, Armante R, Tran H, et al. Temperature dependence of the absorption of the R(6) manifold of the $2\nu_3$ band of methane in air in support of the MERLIN mission. J Quant Spectrosc Radiat Transfer 2023;298:108483. http://dx.doi.org/10.1016/j.jqsrt.2023.108483.

[282] Hilico JC, Loete M, Brown LR. Line strengths of the $\nu_3 - \nu_4$ band of methane. J Mol Spectrosc 1985;111:119–37.

[283] Nassar R, Bernath P. Hot methane spectra for astrophysical applications. J Quant Spectrosc Radiat Transfer 2003;82:279–92.

[284] Hunt RH, Lolck J, Robiette AG, Brown LR, Toth RA. Measurement and analysis of the infrared-absorption spectrum of the $2\nu_2$ band of $^{12}CH_4$. J Mol Spectrosc 1982;92:246–56. http://dx.doi.org/10.1016/0022-2852(82)90097-2.

[285] Pierre G, Champion JP, Guelachvili G, Pascaud E, Poussigue G. Rotational analysis of vibrational polyads in tetrahedral molecules - line parameters of the infrared-spectrum of $^{12}CH_4$ in the range 2250-3260 cm^{-1} - theory versus experiment. J Mol Spectrosc 1983;102:344–60. http://dx.doi.org/10.1016/0022-2852(83)90045-0.

[286] De Martino A, Frey R, Pradere F. Double-resonance observation of the ($3\upsilon_3$, A1) state of methane. Chem Phys Lett 1984;111:113–6. http://dx.doi.org/10.1016/0009-2614(84)80446-7.

[287] De Martino A, Frey R, Pradere F. Double-resonance spectroscopy in methane - theoretical vibration–rotation intensities and experimental investigation of the lower ($3\nu_3$, F_2) level. Mol Phys 1985;55:731–49. http://dx.doi.org/10.1080/00268978500101691.

[288] Pine AS. N_2 and Ar broadening and line mixing in the P and R branches of the ν_3 band of CH_4. J Quant Spectrosc Radiat Transfer 1997;57:157–76. http://dx.doi.org/10.1016/S0022-4073(96)00130-6.

[289] Yousefi M, Bernath PF, Dulick M, Birk M, Wagner G. Line parameters for hot methane ν_3 band broadened by H_2 from 296 to 1100 K. J Quant Spectrosc Radiat Transfer 2021;263:107557. http://dx.doi.org/10.1016/j.jqsrt.2021.107557.

[290] Husson N, Poussigue G, Valentin A, Amiot C. Étude de la bande $\nu_1+\nu_4$ de $^{12}CH_4$ de 4136 à 4288 cm^{-1}. Revue di Phys Appl 1972;7:267–78.

[291] Campargue A, Wang L, Kassi S, Masat M, Votava O. Temperature dependence of the absorption spectrum of CH_4 by high resolution spectroscopy at 81 K: (II) The icosad region (1.49-1.30μm). J Quant Spectrosc Radiat Transfer 2010;111:1141–51. http://dx.doi.org/10.1016/j.jqsrt.2009.11.025.

[292] Margolis JS. Empirical values of the ground state energies for methane transitions between 5500 and 6150 cm^{-1}. Appl Opt 1990;29:2295–302.

[293] Ghysels M, Vasilchenko S, Mondelain D, Beguier S, Kassi S, Campargue A. Laser absorption spectroscopy of methane at 1000 K near 1.7μm: A validation test of the spectroscopic databases. J Quant Spectrosc Radiat Transfer 2018;215:59–70. http://dx.doi.org/10.1016/j.jqsrt.2018.04.032.

[294] Kassi S, Gao B, Romanini D, Campargue A. The near-infrared (1.30-1.70μm) absorption spectrum of methane down to 77 K. Phys Chem Chem Phys 2008;10:4410–9. http://dx.doi.org/10.1039/b805947k.

[295] Wei G, Wei-Dong C, Wei-Jun Z, Yi-Qian Y, Xiao-Ming G. Low temperature laser absorption spectra of methane in the near-infrared at 1.65μm for lower state energy determination. Chinese Phys B 2012;21:014211. http://dx.doi.org/10.1088/1674-1056/21/1/014211.

[296] Yang L, Lin H, Plimmer M, Feng X-J, Chu H-W, Ma Y-J, et al. Possible two-photon absorption in the near-infrared region observed by cavity ring-down spectroscopy. Opt Express 2020;28:39128–36. http://dx.doi.org/10.1364/OE.409421.

[297] Boussin C, Regalia L, Plateaux J, Barbe A. Line intensities and self-broadening coefficients for methane lines between 5500 and 6180 cm^{-1} retrieved with a multispectrum fitting technique. J Mol Spectrosc 1998;191:381–3. http://dx.doi.org/10.1006/jmsp.1998.7647.

[298] Margolis JS. Measured line positions and strengths of methane between 5500 and 6180 cm^{-1}. Appl Opt 1988;27:4038–51.

[299] Gao B, Kassi S, Campargue A. Empirical low energy values for methane transitions in the 5852-6181 cm^{-1} region by absorption spectroscopy at 81 K. J Mol Spectrosc 2009;253:55–63. http://dx.doi.org/10.1016/j.jms.2008.09.005.

[300] Frankenberg C, Warneke T, Butz A, Aben I, Hase F, Spietz P, et al. Pressure broadening in the $2\nu_3$ band of methane and its implication on atmospheric retrievals. Atmos Chem Phys 2008;8:5061–75. http://dx.doi.org/10.5194/acp-8-5061-2008.

[301] Brown LR, Toth RA, Hunt RH, Brault JW. Line assignments and intensities of the $\nu_2 + \nu_3 - \nu_2$ Band of $^{12}CH_4$. J Mol Spectrosc 1981;89:528–41. http://dx.doi.org/10.1016/0022-2852(81)90045-X.

[302] Votava O, Kassi S, Campargue A, Romanini D. Comb coherence-transfer and cavity ring-down saturation spectroscopy around 1.65 : kHz-accurate frequencies of transitions in the $2\nu_3$ band of $^{12}CH_4$. Phys Chem Chem Phys 2022;24:4157–73. http://dx.doi.org/10.1039/d1cp04989e.

[303] de Oliveira VS, Silander I, Rutkowski L, Johansson AC, Soboń G, Axner O, et al. Sub-doppler optical-optical double-resonance spectroscopy of methane using a frequency comb probe, OSA Optical Sensors and Sensing Congress 2021 (AIS, FTS, HISE, SENSORS, ES). 2021, http://dx.doi.org/10.1364/AIS.2021.JTu6E.2, JTu6E.2.

[304] Wang L, Mondelain D, Kassi S, Campargue A. The absorption spectrum of methane at 80 and 294 K in the icosad (6717-7589 cm^{-1}): Improved empirical line lists, isotopologue identification and temperature dependence. J Quant Spectrosc Radiat Transfer 2012;113:47–57. http://dx.doi.org/10.1016/j.jqsrt.2011.09.003.

[305] Malarich NA, Yun D, Sung K, Egbert S, Coburn SC, Drouin BJ, et al. Dual frequency comb absorption spectroscopy of CH_4 up to 1000 Kelvin from 6770 to 7570 cm^{-1}. J Quant Spectrosc Radiat Transfer 2021;272:107812.

[306] Wong A, Bernath PF, Rey M, Nikitin AV, Tyuterev VG. Atlas of experimental and theoretical high-temperature methane cross sections from T=295 to 1000 K in the near-infrared. Astrophys J Suppl 2019;240:4. http://dx.doi.org/10.3847/1538-4365/aaed39.

[307] Masat M, Pracna P, Mondelain D, Kassi S, Campargue A, Votava O. Spectroscopy of jet-cooled methane in the lower icosad region: Empirical assignments of low-J '' spectral lines from two-temperature analysis. J Mol Spectrosc 2013;291:9–15. http://dx.doi.org/10.1016/j.jms.2013.06.002.

[308] Mondelain D, Kassi S, Wang L, Campargue A. The 1.28μm transparency window of methane (7541-7919 cm^{-1}): empirical line lists and temperature dependence (80 k-300 k). Phys Chem Chem Phys 2011;13:7985–96. http://dx.doi.org/10.1039/c0cp02948c.

[309] Singh K, O'Brien JJ. Absorption coefficients for the 727 nm band of methane at 77 K determined by intracavity laser spectroscopy. Astrophys Space Sci 1996;236:97–109. http://dx.doi.org/10.1007/BF00644324.

[310] Beguier S, Kassi S, Campargue A. An empirical line list for methane in the 1.25μm transparency window. J Mol Spectrosc 2015;308:1–5. http://dx.doi.org/10.1016/j.jms.2014.12.020.

[311] Pierre G, Hilico JC, DeBergh C, Maillard JP. The region of the $3\nu_3$ band of methane. J Mol Spectrosc 1980;82:379–93.

[312] Serdyukov VI, Sinitsa LN, Lugovskoi AA, Emel'yanov NM. The $^{12}CH_4$ absorption spectra at 296 K and 200 K in the range between 6000 and 9000 cm^{-1}. In: Matvienko GG, Romanovskii OA, editors. 24th International symposium on atmospheric and ocean optics, atmospheric physics. Proc. SPIE, vol. 10833, SPIE; 2018, http://dx.doi.org/10.1117/12.2504316, 1083309.

[313] Beguier S, Liu AW, Campargue A. An empirical line list for methane near 1μm (9028–10435 cm^{-1}). J Quant Spectrosc Radiat Transfer 2015;166:6–12. http://dx.doi.org/10.1016/j.jqsrt.2015.07.003.

[314] Boraas K, De Boer DF, Lin Z, Reilly JP. The stark effect in methane's $3\nu_1 + \nu_3$ vibrational overtone band. J Chem Phys 1993;99(2):1429–32. http://dx.doi.org/10.1063/1.465388, arXiv:https://pubs.aip.org/aip/jcp/article-pdf/99/2/1429/11039901/1429_1_online.pdf.

[315] Lucchesini A, Gozzini S. Methane diode laser overtone spectroscopy at 840 nm. J Quant Spectrosc Radiat Transfer 2007;103:209–16. http://dx.doi.org/10.1016/j.jqsrt.2006.02.056.

[316] Tsukamoto T, Sasada H. Extended assignments of the $3\nu_1 + \nu_3$ band of methane. J Chem Phys 1995;102:5126–40. http://dx.doi.org/10.1063/1.469238.

[317] Boraas K, Li Z, Reilly JP. High-resolution study of methanes $3\nu_1 + \nu_3$ vibrational overtone band. J Chem Phys 1994;100:7916–27.

[318] Campargue A, Permogorov D, Jost R. Interactivity absorption spectroscopy of the third streching overtone transition of jet cooled methane. J Chem Phys 1995;102:5910–6.

[319] Lucchesini A, Longo I, Gabbanini C, Gozzini S, Moi L. Diode-laser spectroscopy of methane overtone transitions. Appl Opt 1993;32:5211–6. http://dx.doi.org/10.1364/AO.32.005211.

[320] Lucchesini A. Diode laser overtone spectroscopy of methane at 780 nm, arXiv:2202.02187. http://dx.doi.org/10.48550/arXiv.2202.02187.

[321] Singh K, O'Brien JJ. Laboratory measurements of absorption-coefficients for the 727 nm band of methane at 77 K and comparison with results derived from spectra of the giant planets. J Quant Spectrosc Radiat Transfer 1995;54:607–19. http://dx.doi.org/10.1016/0022-4073(95)00102-Q.

[322] Campargue A, Chenevier M, Stoeckel F. Intracavity-laser-absorption spectroscopy of the visible overtone transition of methane in a supersonically cooled jet. Chem Phys Lett 1991;183:153–7.

[323] Campargue A, Karlovets EV, Vasilchenko SS, Turbet M. The high resolution absorption spectrum of methane in the 10 800-14 000 cm^{-1} region: literature review, new results and perspectives. Phys Chem Chem Phys http://dx.doi.org/10.1039/d3cp02385k.